

# VECAMPFIT: vectorized amplitude-analysis fitting library

Kirill Chilikin<sup>a,\*</sup>

<sup>a</sup>*Budker Institute of Nuclear Physics SB RAS, Novosibirsk, Russia*

---

## Abstract

A new library VECAMPFIT for multidimensional amplitude analyses in high-energy physics has been developed for an ongoing amplitude analysis at Belle II experiment. It includes a fitter performing likelihood calculation and explicitly-vectorized subprograms for amplitude implementation. The fitter supports explicit gradient calculation and simultaneous fitting of multiple data sets.

*Keywords:* Amplitude analysis

---

## PROGRAM SUMMARY

*Program Title:* VECAMPFIT

*Developer's repository link:* <https://gitlab.desy.de/chilikin/vecampfit>

*Licensing provisions:* Apache License, Version 2.0

*Programming language:* Fortran, C++, C

*Nature of problem:* Amplitude analyses require a large amount of calculations, especially for evaluation of signal-density normalization integrals. Thus, optimization of amplitude-analysis fitting programs is important for efficient data analysis at high-energy-physics experiments.

*Solution method:* VECAMPFIT library is designed to achieve high performance of the analysis code by vectorization of data storage and amplitude calculations, providing a number of vectorized subroutines for physical quantities and mathematical functions, and calculation of likelihood gradient. Parallel calculations are possible using OPENMP.

---

\*Corresponding author.

*E-mail address:* K.A.Chilikin@inp.nsk.su

## 1. Introduction

### 1.1. Amplitude analyses and their computational requirements

Particle decays, reactions between the beam and target, or beam-annihilation processes are described by their complex amplitude. The general form of the signal density for particle decays is

$$S(\Phi, p_S) = \sum_f \sum_{ij} \rho_{ij} \left[ \sum_k A_{ikf}(\Phi, p_S) \right] \left[ \sum_{k'} A_{jk'f}^*(\Phi, p_S) \right] \quad (1)$$

where  $\Phi$  is the decay phase space,  $p_S$  are signal-density parameters,  $i$  and  $j$  are the initial state,  $k$  and  $k'$  are the intermediate state,  $f$  is the final state,  $\rho$  is the initial-state density matrix,  $A$  is the decay amplitude, and asterisk denotes complex conjugation. Fitting experimental-data events to signal-density expressions similar to Eq. (1) is referred to as amplitude analysis. Its simplest case is an analysis of a three-body decay of a spin-zero particle such as  $B$  or  $D$  which is referred to as a Dalitz analysis and corresponds to a two-dimensional phase space, which may be represented, for example, as two squared invariant masses of the final-state particle pairs  $m_{12}^2$  and  $m_{23}^2$ .

For more complex cases, the decay phase space has more than two dimensions. Such decays have four or more final-state particles e.g.  $D^0 \rightarrow K^- \pi^+ \pi^+ \pi^-$ , possibly including subsequent decays of relatively narrow states e.g.  $B^+ \rightarrow J/\psi(\rightarrow \mu^+ \mu^-) \phi(\rightarrow K^+ K^-) K^+$ , or additional angular dependence due to non-zero spin of the initial particle, e.g.  $e^+ e^- \rightarrow K^+ K^- \pi^0$ . Amplitude analyses of the decays with three or more phase-space dimensions are referred to as multidimensional. Multidimensional amplitude analysis is the most sensitive method for analyzing complex decay chains since it allows to use all available information about the dependency of the signal density on the phase-space variables. Such analyses provide many interesting physics results. Some examples from the field of quarkonium spectroscopy, which motivated this work, include determination of the  $\chi_{c1}(3872)$  quantum numbers [1, 2], studies of the  $T_{c\bar{c}1}(4430)^+$  [3, 4], observation of multiple exotic states in  $B^+ \rightarrow J/\psi \phi K^+$  [5, 6], determination of the  $T_{b\bar{b}1}(10610)^+$  and  $T_{b\bar{b}1}(10650)^+$  quantum numbers [7], and others.

In a real experiment, the probability density function of the observed events corresponding to the signal density given by Eq. (1) is modified by

the detection efficiency, resolution, and presence of background:

$$\begin{aligned} \rho(\Phi, p_S, p_B) = & f_S \frac{\int R(\Phi, \Phi') \epsilon(\Phi') S(\Phi', p_S) d\Phi'}{\int \int R(\Phi, \Phi') \epsilon(\Phi') S(\Phi', p_S) d\Phi' d\Phi} \\ & + \sum_k f_B^{(k)} \frac{\epsilon(\Phi) B^{(k)}(\Phi, p_B^{(k)})}{\int \epsilon(\Phi) B^{(k)}(\Phi, p_B^{(k)}) d\Phi}, \end{aligned} \quad (2)$$

where  $\Phi'$  is the phase space for true kinematic parameters,  $\Phi$  is the phase space for reconstructed kinematic parameters,  $f_S$  is the signal fraction,  $k$  is the number of the background source,  $f_B^{(k)}$  is the background fraction,  $R$  is the resolution function,  $\epsilon$  is the signal detection efficiency,  $B^{(k)}$  is the background density, and  $p_B^{(k)}$  are the background-density parameters. Here the background density function is defined so that it needs to be multiplied by the signal efficiency to get the actual background distribution:

$$B_{(\text{obs})}^{(k)}(\Phi, p_B^{(k)}) = B^{(k)}(\Phi, p_B^{(k)}) \epsilon(\Phi), \quad (3)$$

where  $B_{(\text{obs})}^{(k)}$  is the observed background distribution. It is not necessary to parameterize the efficiency if this background-density definition is used. Although usually a single background density function is used, multiple background sources may be necessary, for example, if a specific peaking-background source is described from Monte Carlo (MC) simulation, while the remaining background is described by its distribution in a control region.

The resolution term vanishes in the signal normalization integral after performing integration over  $\Phi$  first:

$$\begin{aligned} \rho(\Phi, p_S, p_B) = & f_S \frac{\int R(\Phi, \Phi') \epsilon(\Phi') S(\Phi', p_S) d\Phi'}{\int \epsilon(\Phi') S(\Phi', p_S) d\Phi'} \\ & + \sum_k f_B^{(k)} \frac{\epsilon(\Phi) B^{(k)}(\Phi, p_B^{(k)})}{\int \epsilon(\Phi) B^{(k)}(\Phi, p_B^{(k)}) d\Phi}. \end{aligned} \quad (4)$$

Unbinned maximum-likelihood fits are performed using this general density-function form as discussed in more detail in Sec. 2. The background density is often determined from a control region before the signal fit, although simultaneous fitting of the background and signal regions is also possible. In this case the background normalization integral needs to be calculated only one

time before the fit. The signal normalization integral needs to be calculated for each likelihood-function call.

In case of the isobar model (coherent sum of individual-resonance amplitudes) the amplitude can be represented in the following form:

$$A = \sum_k a_{ikf} R_{ikf}(\Phi, p_S), \quad (5)$$

where  $a_{ikf}$  are complex amplitudes and  $R_{ikf}(\Phi, p_S)$  are resonant shapes for the initial state  $i$ , intermediate state  $k$ , and final state  $f$ . If the parameters of intermediate resonances are not varied, the signal normalization integral reduces to

$$\sum_f \sum_{ij} \rho_{ij} \sum_{k,k'} a_{ikf} a_{jk'f}^* \int \epsilon(\Phi) R_{ikf}(\Phi, p_S) R_{jk'f}^*(\Phi, p_S) d\Phi, \quad (6)$$

where all integrals need to be calculated only once. Generally, however, such reduction is impossible. If the lineshape of any individual contribution is determined from the fit, then full integration needs to be performed at each minimization step.

This necessity of numeric calculation of the signal-density integral results in fitting programs requiring a large processing time. Their optimization is important for efficient experimental data analysis. The optimization is a common task for multiple physics analyses, as integration methods and various amplitude expressions are common for different analyses. This motivates development of specialized amplitude-analysis frameworks.

### 1.2. Optimization methods and implementation approaches

There are several possible ways to reduce the fitting time. The first one is optimization of the density-function calculation. The density-function implementation needs to avoid any unnecessary calculations. Values depending on the phase-space point but not fit parameters such as angular distributions need to be calculated in advance and stored in buffers. Similarly, values depending on fit parameters only need to be calculated at the beginning of each likelihood-function call. Finally, the calculation should avoid any conditional checks such as whether a resonance is included into the model if it is possible to perform such checks at compilation time. Another way of calculation optimization is usage of hardware parallelism. One can use the fact that both data events and normalization integrals require computation of the

same density function for a large number of phase-space points and utilize single-instruction multiple-data (SIMD) code. SIMD instructions perform the same operation for each element of a fixed-length vector register.

The second method is optimization of the minimization procedure. Gradient-minimization algorithms such as the Fletcher’s algorithm [8] known as MI-GRAD in MINUIT [9] perform calculations of gradient and Hessian. Both gradient and Hessian can be calculated symbolically or obtained from the signal-density functions by automatic differentiation algorithms, and then used by the minimization instead of the results of numerical calculations. The function calls with gradient calculation take a longer time but the necessary number of the calls becomes lower.

Finally, the execution time of a single fit can be reduced by performing parallel calculations. The parallel calculations can be performed using multiple threads on the same machine, for example, via OpenMP [10]. Another way is to perform parallel calculations with different processes on different machines; the process communication can be implemented using OpenMPI [11]. Finally, one can use offloading to GPUs, which also perform calculations in parallel, for example, via OpenACC [12].

There are two different approaches to amplitude-analysis programming. In the classical imperative-programming approach, the amplitude or signal density is implemented as a function in an imperative language such as C++ or Fortran. The amplitude may also be created dynamically from explicitly-programmed amplitudes of individual contributions using a model class or configuration file. Examples of imperative amplitude-analysis frameworks include LAURA<sup>++</sup> [13], AMPTOOLS [14], PAWIAN [15]. In the declarative-programming approach, the amplitude is specified as a mathematical function, and the exact operations are prepared by a computational backend or code-generation program rather than programmed explicitly. Since similar programming techniques are commonly used in machine learning, several declarative-programming frameworks are based on TENSORFLOW [16]; their examples include TENSORFLOWANALYSIS2 [17] and TF-PWA [18]. ComPWA project [19] can use several computational backends including JAX [20], NUMPY [21], and TENSORFLOW. The amplitude generator AMPGEN [22] works in a different way and generates C++ code for isobar-model amplitudes in accordance with their description in the framework’s own format. Complete AMPGEN-based source code is available for LHCb  $B^+ \rightarrow \psi(2S)K^+\pi^+\pi^-$  analysis [23, 24].

Generally, the declarative-programming approach results in easier opti-

mization from the user point of view, since the vectorization and gradient calculation can be performed by a framework in the functional form if it supports them, but implementation of the framework itself requires more effort. In case of imperative programming, the vectorization and gradient calculation need to be implemented explicitly.

### 1.3. VECAMPFIT *library*

VECAMPFIT is a new fitting framework developed for an ongoing multidimensional amplitude analysis at Belle II experiment [25]. It is a continuation of amplitude-analysis work performed at Belle [26, 27] and Belle II since 2009 but no existing analysis is based on the library yet. VECAMPFIT is not limited to any specific model, instead, it is a library implementing a fitter and functions necessary to build the amplitude; the signal and background density functions need to be programmed by the user. VECAMPFIT is written in the imperative-programming approach, taking effort to overcome its performance limitations. Mixed-language programming is used: the amplitude calculation is implemented in Fortran 2018, while the general fit control is performed by C++ code. All VECAMPFIT subprograms intended to be used in amplitudes are vectorized and operate on short data vectors of a fixed length. This is the origin of the library name. Values depending on the phase-space point are stored in vectorized buffers; values depending on fit parameters only can also be bufferized. Configuration is performed at compilation time by preprocessor. The fitters supports minimization with explicit calculation of gradient, which needs to be calculated and implemented by the user (automatic differentiation is not supported), but not all library subprograms have versions with gradient calculation yet. Thread-level parallel calculations are possible using OpenMP, but parallel calculations on different machines using OpenMPI are not supported. Offloading to GPUs is currently experimental. It works for calculation of signal density function without explicit gradient calculation and requires a compiler that can perform offloading using OpenACC.

VECAMPFIT consists of several parts. Fortran processing tool `vecampfit-fortran` is used during building for automatic generation of Fortran interfaces, C headers, and documentation. The library `vecampfit-real` contains subprograms for operations on representation of real numbers such as extraction or setting of the mantissa, transfer and type-conversion functions for integer and real numbers. The library `vecampfit-arbitrary-precision` implements integer arithmetic, operations on arbitrary-precision integer, real,

and complex numbers, and functions calculated using arbitrary-precision arithmetics. The arbitrary-precision operations are used to calculate mathematical constants such as  $e$  or  $\pi$  and series coefficients used in implementation of vectorized functions.

The main library `vecampfit` contains the implementation of the basic complex-vector type, mathematical constants and functions, interpolation, linear algebra, numeric integration, statistical functions and tests, physical functions useful for implementation of amplitudes related to kinematics, high-energy physics, and quantum mechanics, functions for generation of Monte Carlo events, particle data, ROOT interface [28], and the fitter. In addition, it implements specialized neural networks used for parameterization of efficiency and background distributions, which are experimental and are not described here.

Amplitude-analysis formalism is described in Sec. 2. Example of  $D^0 \rightarrow K^- \pi^+ \pi^0$  Dalitz analysis is then presented in Sec. 3. This example is used to describe the details of implementation of the amplitude-analysis formalism in VECAMPFIT in Sec. 4 and fitting procedure in Sec. 5. VECAMPFIT auxiliary parts and subprograms intended for implementation of density functions are described in Sec. 6. A complex example of analysis workflow including efficiency, resolution, background, and signal fits is presented in Sec. 7 using a simultaneous fit of the processes  $e^+e^- \rightarrow K^+K^-\pi^+\pi^-$  and  $e^+e^- \rightarrow K_S^0 K_S^0 \pi^+ \pi^-$  at multiple beam energies. Performance studies are presented in Sec. 8.

## 2. Amplitude-analysis formalism

### 2.1. Unbinned maximum-likelihood fit

If resolution can be ignored, one can set  $R(\Phi, \Phi') = \delta(\Phi, \Phi')$  and the probability density given by Eq. (4) becomes

$$\rho(\Phi, p_S, p_B) = f_S \frac{\epsilon(\Phi) S(\Phi, p_S)}{\int \epsilon(\Phi) S(\Phi, p_S) d\Phi} + \sum_k f_B^{(k)} \frac{\epsilon(\Phi) B^{(k)}(\Phi, p_B^{(k)})}{\int \epsilon(\Phi) B^{(k)}(\Phi, p_B^{(k)}) d\Phi}. \quad (7)$$

If the resolution cannot be ignored, then it is necessary to perform convolution of the signal density and resolution numerically. Fitting with resolution is not supported in VECAMPFIT yet.

In case of a standard maximum-likelihood fit which does not determine the normalization, the background fractions  $f_B^{(k)}$  are fit parameters and the

signal fraction  $f_S$  is calculated as

$$f_S = 1 - \sum_k f_B^{(k)}. \quad (8)$$

In case of an extended maximum-likelihood fit, the signal yield  $N_S$  and background yields  $N_B^{(k)}$  are fit parameters. The fractions are given by

$$f_S = \frac{N_S}{N}, \quad f_B^{(k)} = \frac{N_B^{(k)}}{N}, \quad (9)$$

where  $N$  is the total yield given by

$$N = N_S + \sum_k N_B^{(k)}. \quad (10)$$

The probability density for the yield is given by the Poisson distribution

$$\rho(N) = \frac{N^{N_{\text{data}}} \exp(-N)}{\Gamma(N_{\text{data}} + 1)}, \quad (11)$$

where  $N_{\text{data}}$  is the number of observed data events and factorial is replaced by equivalent  $\Gamma$  function to use  $\ln \Gamma$  for logarithm calculation.

The number of background sources is set by the user; the default number is zero. The background density has to be predetermined from a separate fit; variation of the background parameters during signal fit is not supported. The background fractions  $f_B^{(k)}$  or yields  $N_B^{(k)}$  should be fit parameters; their numbers needs to be set by the user for each background source before loading of fit data. The background-fraction parameter may either be set entirely free or constrained from a separate fit, for example, to the invariant mass of the parent particle or the difference between the reconstructed energy and half of beam energy  $\Delta E = E - \sqrt{s}/2$  in case of production of a particle-antiparticle pair at a  $e^+e^-$  collider.

Three ways of calculation of the normalization integral  $\int \epsilon(\Phi)S(\Phi)d\Phi$  are implemented in VECAMPFIT: Monte Carlo, grid, and formula integration. In addition, calculation of the normalization integral can be disabled. The integration method can be set by calling `vecampfit_fitter_set_normalization_integration_type()`; the default method is MC integration.

### 2.1.1. Monte Carlo integration

In case of MC integration, the normalization integrals are calculated using MC events. The MC events are generated using some density function  $d_{\text{MC}}(\Phi)$  and then passed through detector simulation, which changes their distribution to  $d_{\text{MC}}(\Phi)\epsilon(\Phi)$ . While common first choice is the uniform distribution  $d_{\text{MC}}(\Phi) = 1$ , it is recommended to increase the number of events in the regions of higher signal density such as narrow resonances or regions of rapid signal-density change such as  $\rho$ - $\omega$  interference to improve integration precision.

The signal normalization integral is given by

$$\int \epsilon(\Phi)S(\Phi, p_S)d\Phi = \frac{\bar{\epsilon}}{N_{\text{MC}}} \sum_j w_j S(\Phi_j, p_S), \quad (12)$$

where

$$\bar{\epsilon} = \int \epsilon(\Phi)d\Phi, \quad (13)$$

$N_{\text{MC}}$  is the number of MC events, the index  $j$  runs over normalization MC events, and  $w_j$  are MC weights. The weights need to be assigned by the user and their choice is not restricted by the library. It is necessary to take into account the density function used for generation:

$$w_j \propto \frac{1}{d_{\text{MC}}(\Phi_j)}, \quad (14)$$

but the weights may also include other effects such as the difference of the efficiency between the data and MC. The weights may be scaled arbitrarily as their multiplication by a common constant adds a constant to the likelihood function and does not affect the fit results.

Example weight definition taking the difference of the efficiency between the data and MC into account is

$$w_j = \frac{R(\Phi_j)}{d_{\text{MC}}(\Phi_j)}, \quad (15)$$

where  $R(\Phi_j)$  is the ratio between the efficiencies in data and MC, which can be determined as

$$R(\Phi) = \prod_k \frac{\epsilon_{\text{data}}^{(k)}(\Phi)}{\epsilon_{\text{MC}}^{(k)}(\Phi)}, \quad (16)$$

where  $k$  is the final-state particle index,  $\epsilon_{\text{data}}^{(k)}$  and  $\epsilon_{\text{MC}}^{(k)}$  are the efficiencies in data and MC, respectively. The efficiency ratios for individual final-state particles need to be determined from control samples.

The function to be minimized for an unbinned maximum-likelihood fit is

$$\mathcal{F} = \sum_i -2 \ln \left[ f_S \frac{S(\Phi_i, p_S)}{\sum_j w_j S(\Phi_j, p_S)} + \sum_k f_B^{(k)} \frac{B^{(k)}(\Phi_i, p_B^{(k)})}{\sum_j w_j B^{(k)}(\Phi_j, p_B^{(k)})} \right] - 2 \ln \frac{\epsilon(\Phi_i) N_{\text{MC}}}{\bar{\epsilon}}, \quad (17)$$

where the index  $i$  runs over data events. The second logarithm in Eq. (17) is constant and it can be omitted. The VECAMPFIT implementation provides also a way to add data weights  $w_i$  and parameter prior likelihoods:

$$\mathcal{F} = \sum_i -2w_i \ln \left[ f_S \frac{S(\Phi_i, p_S)}{\sum_j w_j S(\Phi_j, p_S)} + \sum_k f_B^{(k)} \frac{B^{(k)}(\Phi_i, p_B^{(k)})}{\sum_j w_j B^{(k)}(\Phi_j, p_B^{(k)})} \right] + \sum_l C_l(p_S^{(n_l)}) + C(p_S), \quad (18)$$

where  $l$  is the prior-likelihood number,  $n_l$  is the parameter number for  $l$ -th prior-likelihood,  $C_l$  is a library-defined prior-likelihood function, and  $C$  is a user-defined prior-likelihood function. A common case of asymmetric-Gaussian prior likelihoods is implemented in the library:

$$C_l(p_S^{(n_l)}) = \begin{cases} \left( \frac{p_S^{(n_l)} - (p_S^{(n_l)})_{(0)}}{\sigma_{n_l}^{(-)}} \right)^2 & \text{for } p_S^{(n_l)} < (p_S^{(n_l)})_{(0)}, \\ \left( \frac{p_S^{(n_l)} - (p_S^{(n_l)})_{(0)}}{\sigma_{n_l}^{(+)}} \right)^2 & \text{for } p_S^{(n_l)} \geq (p_S^{(n_l)})_{(0)}, \end{cases} \quad (19)$$

where  $(p_S^{(n_l)})_{(0)}$  is the central value, and  $\sigma_{n_l}^{(-)}$  and  $\sigma_{n_l}^{(+)}$  are the negative-side and positive-side standard deviations, respectively. The data weights are usually not necessary for actual amplitude analysis, but they are needed, for example, for parameterization of a background originating from a specific channel using its signal MC events to take the difference between the reconstruction efficiency in data and MC into account. Errors returned by the fit are not correct if fitting with the data weights and they need to be estimated separately from pseudoexperiments.

In case of extended unbinned maximum likelihood fit the likelihood has an additional term

$$\Delta\mathcal{F} = -2 \ln \frac{N^{N_{\text{data}}} \exp(-N)}{\Gamma(N_{\text{data}} + 1)} = 2(N - N_{\text{data}} \ln(N)), \quad (20)$$

where the constant term containing the logarithmic  $\Gamma$  function is omitted.

The fit can also be performed simultaneously for several data sets. The likelihood function is then

$$\begin{aligned} \mathcal{F} = \sum_a \sum_i -2w_i \ln & \left[ (f_S)_a \frac{S_a(\Phi_i, p_S)}{\sum_j w_j S_a(\Phi_j, p_S)} + \sum_k (f_B^{(k)})_a \frac{B_a^{(k)}(\Phi_i, p_B^{(k)})}{\sum_j w_j B_a^{(k)}(\Phi_j, p_B^{(k)})} \right] \\ & + \sum_l C_l(p_S^{(n_l)}) + C(p_S), \end{aligned} \quad (21)$$

where  $a$  is the number of simultaneous-fit point, and the signal density  $S_a$ , the background densities  $B_a^{(k)}$ , the signal fraction  $(f_S)_a$ , and the background fractions  $(f_B^{(k)})_a$  all depend on the simultaneous-fit point.

An alternative approach is to parameterize the efficiency  $\epsilon(\Phi)$  by a separate procedure and use MC points without detector simulation for fitting. This is equivalent to redefinition of the signal and background density functions:

$$\begin{aligned} S_\epsilon(\Phi, p_S) &= S(\Phi, p_S)\epsilon(\Phi), \\ B_\epsilon^{(k)}(\Phi, p_B^{(k)}) &= B^{(k)}(\Phi, p_B^{(k)})\epsilon(\Phi) = B_{(\text{obs})}^{(k)}(\Phi, p_B^{(k)}). \end{aligned} \quad (22)$$

The ratio between the efficiencies in data and MC  $R(\Phi_j)$  is supposed to be taken into account when parameterizing the efficiency in this case; however, the weights related to non-uniform MC density function  $d_{\text{MC}}(\Phi)$  still remain. The likelihood becomes

$$\begin{aligned} \mathcal{F} = \sum_i -2w_i \ln & \left[ f_S \frac{S_\epsilon(\Phi_i, p_S)}{\sum_j w_j S_\epsilon(\Phi_j, p_S)} + \sum_k f_B^{(k)} \frac{B_\epsilon^{(k)}(\Phi_i, p_B^{(k)})}{\sum_j w_j B_\epsilon^{(k)}(\Phi_j, p_B^{(k)})} \right] \\ & + \sum_l C_l(p_S^{(n_l)}) + C(p_S). \end{aligned} \quad (23)$$

VECFIT does not provide any special support for fitting with parameterized efficiency, however, since the likelihood formula is almost the same

as Eq. (18), such fit can be performed by the user with the existing fitter code after redefinition of the signal density function as given by Eq. (22) and appropriate redefinition of weights. Redefinition of the background-density parameterization is not necessary but it is needs to be fitted using the same MC as for the signal fit.

### 2.1.2. Grid integration

The likelihood for grid integration is the same as the likelihood for MC integration with parameterized efficiency given by Eq. (23), but the definitions of weights and integration points are different. In case of the grid integration, the index  $j$  runs over grid points which need to be defined by the user in the fitting program. The weights are given by

$$w_j = w_j^{(\text{integration})} w_j^{(\text{Jacobian})}, \quad (24)$$

where  $w_j^{(\text{integration})}$  are weights originating from the integration method and  $w_j^{(\text{Jacobian})}$  are weights originating from the Jacobian of the transformation between the phase-space and grid coordinates.

For example, Gauss-Legendre quadrature is used for integration in the  $B^+ \rightarrow K^+ K^+ K^-$  example described in Sec. 8.2; the integration weights are the Gauss-Legendre weights rescaled by the size of the integration region:

$$w_{j_1 j_2}^{(\text{integration})} = \frac{m_{K_1^+ K^-}^{(\text{max})} - m_{K_1^+ K^-}^{(\text{min})}}{2} \frac{m_{K_2^+ K^-}^{(\text{max})} - m_{K_2^+ K^-}^{(\text{min})}}{2} w_{j_1}^{(\text{GL})} w_{j_2}^{(\text{GL})}, \quad (25)$$

where the indices  $n = 1, 2$  correspond to the number of  $K^+$ ,  $m_{K_n^+ K^-}^{(\text{max})}$  and  $m_{K_n^+ K^-}^{(\text{min})}$  are the maximum and minimum invariant masses in the integration range, respectively, and  $w_{j_n}^{(\text{GL})}$  are Gauss-Legendre weights for integration over the interval  $[-1, 1]$ . The grid is defined in invariant-mass coordinates, thus

$$w_j^{(\text{Jacobian})} = \frac{\partial m_{K_1^+ K^-}^2}{\partial m_{K_1^+ K^-}} \frac{\partial m_{K_2^+ K^-}^2}{\partial m_{K_2^+ K^-}} = 4m_{K_1^+ K^-} m_{K_2^+ K^-}. \quad (26)$$

The minimum and maximum invariant masses do not have to be the same as the kinematic borders of the Dalitz plot because it may be split into several integration regions.

### 2.1.3. Formula integration

In case of formula integration, the normalization integrals in Eq. (7) are calculated symbolically. This method can only work for simple fits that do not require to take the efficiency into account. Formula integration is only supported for fits without background. Thus, the probability density is

$$\rho(\Phi, p_S) = \frac{S(\Phi, p_S)}{\int S(\Phi, p_S) d\Phi} \quad (27)$$

in case of formula integration. If this method is used, then the user has to calculate the integral and provide the integration function by calling `vecampfit_fitter_set_integration_function()`. The integration function  $I(p_S)$  should only depend on fit parameters:

$$I(p_S) = \int S(\Phi, p_S) d\Phi. \quad (28)$$

### 2.1.4. Fit without normalization

Finally, the calculation of the normalization integral can be disabled. This is necessary in certain specific cases. For example, one can fit reconstruction efficiency using generator-level MC events defining the probability density function as

$$\rho(\Phi) = \begin{cases} \epsilon(\Phi) & \text{for reconstructed events,} \\ 1 - \epsilon(\Phi) & \text{for non-reconstructed events.} \end{cases} \quad (29)$$

The function defined in this way does not need any further normalization.

## 2.2. Fit with explicit gradient calculation

The likelihood function for Monte Carlo integration is given by Eq. (18). Partial derivatives of the likelihood are

$$\begin{aligned} \frac{\partial \mathcal{F}}{\partial p_S^{(\alpha)}} = & \sum_i \frac{-2f_S w_i}{f_S \sum_j \frac{S(\Phi_i, p_S)}{w_j S(\Phi_j, p_S)} + \sum_k f_B^{(k)} \frac{B^{(k)}(\Phi_i, p_B^{(k)})}{\sum_j w_j B^{(k)}(\Phi_j, p_B^{(k)})}} \\ & \times \left[ \frac{\frac{\partial S(\Phi_i, p_S)}{\partial p_S^{(\alpha)}}}{\sum_j w_j S(\Phi_j, p_S)} - \frac{S(\Phi_i, p_S)}{\left(\sum_j w_j S(\Phi_j, p_S)\right)^2} \left(\sum_j w_j \frac{\partial S(\Phi_j, p_S)}{\partial p_S^{(\alpha)}}\right) \right] \\ & + \delta_{n_k \alpha} \frac{\partial C_k(p_S^{(n_k)})}{\partial p_S^{(\alpha)}} + \frac{\partial C(p_S)}{\partial p_S^{(\alpha)}}, \end{aligned} \quad (30)$$

where  $\alpha$  is the parameter number. Since the derivatives depend on the signal-density derivatives, it is necessary to calculate not only the signal density, but also the gradient  $\partial S(\Phi, p_S)/\partial p_S^{(\alpha)}$  for each data and MC event. Two signal density functions need to be set, the first one computing both signal density and its gradient simultaneously, and the second one computing the signal density only. Partial derivatives of the likelihood over the signal and background fractions are

$$\begin{aligned} \frac{\partial \mathcal{F}}{\partial f_S} = & \sum_i \frac{-2 \frac{S(\Phi_i, p_S)}{\sum_j w_j S(\Phi_j, p_S)} w_i}{f_S \sum_j \frac{S(\Phi_i, p_S)}{w_j S(\Phi_j, p_S)} + \sum_k f_B^{(k)} \frac{B^{(k)}(\Phi_i, p_B^{(k)})}{\sum_j w_j B^{(k)}(\Phi_j, p_B^{(k)})}}, \\ \frac{\partial \mathcal{F}}{\partial f_B^{(k)}} = & \sum_i \frac{-2 \frac{B^{(k)}(\Phi_i, p_B)}{\sum_j w_j B^{(k)}(\Phi_j, p_B)} w_i}{f_S \sum_j \frac{S(\Phi_i, p_S)}{w_j S(\Phi_j, p_S)} + \sum_k f_B^{(k)} \frac{B^{(k)}(\Phi_i, p_B^{(k)})}{\sum_j w_j B^{(k)}(\Phi_j, p_B^{(k)})}}. \end{aligned} \quad (31)$$

In case of a standard maximum likelihood fit, the signal fraction is calculated from background fractions using Eq. (8), thus, it is necessary to subtract the partial derivative over the signal fraction from the background ones:

$$\frac{\partial \mathcal{F}}{\partial f_B^{(k)}} \rightarrow \frac{\partial \mathcal{F}}{\partial f_B^{(k)}} - \frac{\partial \mathcal{F}}{\partial f_S}. \quad (32)$$

In case of extended unbinned maximum likelihood fit, yields are fit parameters. After addition of the extended-likelihood term derivatives, the yield derivatives are given by

$$\begin{aligned}\frac{\partial \mathcal{F}}{\partial N_S} &= 2 + \frac{1}{N} \sum_i \frac{\partial \mathcal{F}}{\partial f_S}, \\ \frac{\partial \mathcal{F}}{\partial N_B^{(k)}} &= 2 + \frac{1}{N} \sum_i \frac{\partial \mathcal{F}}{\partial f_B^{(k)}}.\end{aligned}\tag{33}$$

### 3. $D^0 \rightarrow K^- \pi^+ \pi^0$ Dalitz analysis example

The  $D^0 \rightarrow K^- \pi^+ \pi^0$  Dalitz analysis based on CLEO model [29]. As for any Dalitz analysis, the amplitude is defined in a two-dimensional phase space  $\Phi = (M_{K^- \pi^+}^2, M_{K^- \pi^0}^2)$ . The decays of intermediate resonances are described by the Breit-Wigner amplitude

$$\begin{aligned}B_R^{(\text{no } q)}(m) &= \frac{\frac{F_R(q)}{F_R(q_0)}}{m_0^2 - m^2 - im_0 \Gamma(m)}, \\ \Gamma(m) &= \Gamma_0 \left( \frac{q}{q_0} \right)^{2L+1} \frac{m_0}{m} \frac{F_R^2(q)}{F_R^2(q_0)},\end{aligned}\tag{34}$$

where  $R$  is the decaying resonance,  $m_0$  and  $\Gamma_0$  are its mass and width, respectively,  $m = \sqrt{s}$  is the invariant mass,  $q$  and  $q_0$  are the daughter momenta for the invariant and resonance masses, respectively,  $L$  is the angular momentum, and  $F_R(q)$  and  $F_R(q_0)$  are the formfactors at the invariant and resonance masses, respectively. The superscript “(no  $q$ )” refers to the absence of a phase-space factor in the numerator. Blatt-Weisskopf formfactors [30] are used:

$$F_R^{(\text{BW})}(q, r, L) = \frac{1}{\sqrt{|h_L^{(1)}(z)|z^{L+1}}},\tag{35}$$

where  $r$  is the effective radius,  $z = qr$  and  $h_L^{(1)}(z)$  is the spherical Hankel function of the first kind. For particular values of the angular momentum  $L$ ,

the Blatt-Weisskopf formfactors are

$$\begin{aligned}
F_R^{(\text{BW})}(q, r, 0) &= 1, \\
F_R^{(\text{BW})}(q, r, 1) &= \frac{1}{\sqrt{z^2 + 1}}, \\
F_R^{(\text{BW})}(q, r, 2) &= \frac{1}{\sqrt{z^4 + 3z^2 + 9}}, \\
F_R^{(\text{BW})}(q, r, 3) &= \frac{1}{\sqrt{z^6 + 6z^4 + 45z^2 + 225}}, \\
F_R^{(\text{BW})}(q, r, 4) &= \frac{1}{\sqrt{z^8 + 10z^6 + 135z^4 + 1575z^2 + 11025}}, \\
F_R^{(\text{BW})}(q, r, 5) &= \frac{1}{\sqrt{z^{10} + 15z^8 + 315z^6 + 6300z^4 + 99225z^2 + 893025}}.
\end{aligned} \tag{36}$$

The amplitude is calculated using covariant formalism. The result is

$$A(\Phi) = a_{nr} e^{i\phi_{nr}} + \sum_R a_{Rr} e^{i\phi_R} \frac{F_D^{(\text{BW})}(q, r^{(D)}, J)}{F_D^{(\text{BW})}(q_0, r^{(D)}, J)} B_R^{(\text{no } q)}(M_{AB}) \mathcal{A}_J(ABC|R) \tag{37}$$

where  $q$  and  $q_0$  are the momenta of the decay  $D \rightarrow RC$  ( $R$  being an intermediate resonance in the  $AB$  system) for the invariant mass of the combination  $AB$  and the mass of the intermediate resonance  $R$ , respectively,  $r^{(D)}$  is the  $D$  effective radius,  $J$  is the  $R$  spin, and the angular part is

$$\begin{aligned}
\mathcal{A}_0(ABC|R) &= 1; \\
\mathcal{A}_1(ABC|R) &= M_{AC}^2 - M_{BC}^2 + \frac{(M_D^2 - M_C^2)(M_B^2 - M_A^2)}{M_R^2}.
\end{aligned} \tag{38}$$

Depending on the intermediate combination, the following particle orders are used:  $(A, B, C) = (\pi^+, \pi^0, K^-)$ ,  $(K^-, \pi^+, \pi^0)$ ,  $(K^-, \pi^0, \pi^+)$ . Since all initial and final-state particles have zero spin, the signal density function is  $S(\Phi) = |A(\Phi)|^2$ .

The model includes 7 resonances:  $\rho(770)^+$  and  $\rho(1700)^+$  decaying to  $\pi^+\pi^0$ ;  $K^*(892)^-$ ,  $K_0^*(1430)^-$ , and  $K^*(1680)^-$  decaying to  $K^-\pi^0$ ;  $\bar{K}^*(892)^0$  and  $\bar{K}_0^*(1430)^0$  decaying to  $K^-\pi^+$ . The  $D^0$  is below the threshold of the decay  $D^0 \rightarrow \rho(1700)^+ K^-$  for the  $\rho(1700)^+$  nominal mass, thus, the formfactor normalization to unity at the nominal mass is impossible. Since no other method is described by CLEO, the exact normalization used for the  $\rho(1700)^+$

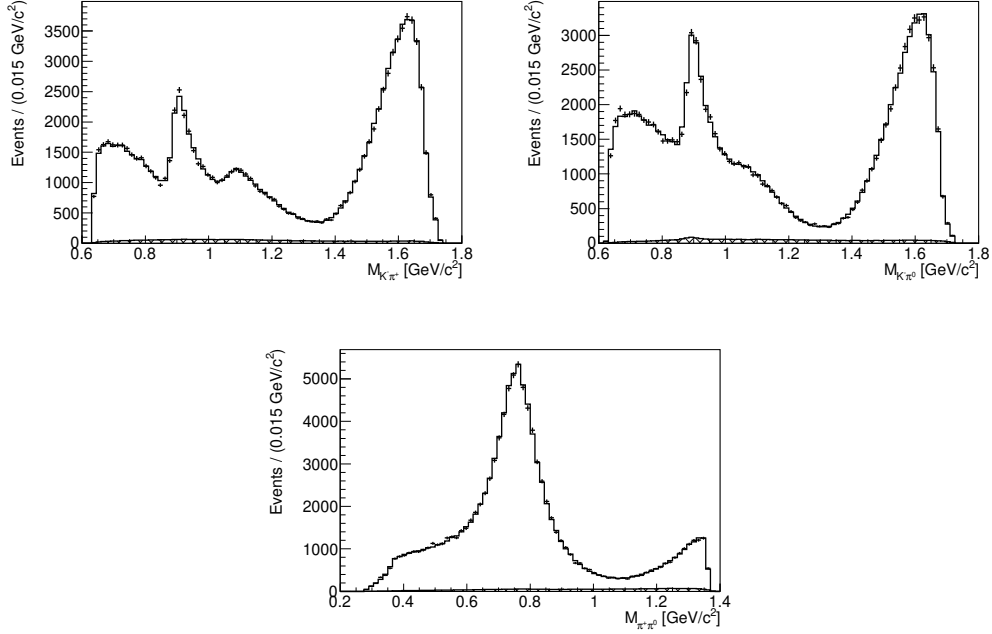


Figure 1: Results of fit to the  $D^0 \rightarrow K^- \pi^+ \pi^0$  signal distribution for a pseudoexperiment. The points with error bars are data, the solid line is the fit result, and the hatched histograms are the background contribution.

cannot be recovered. In the VECAMPFIT example, the normalization form-factor  $F_D^{(\text{BW})}(q_0, r^{(D)}, J)$  is simply omitted for the  $\rho(1700)^+$ . The results of CLEO fit are used as the default values for MC generation. Results of the fit to a pseudoexperiment with 100000 signal events are shown in Fig. 1. The example does not include reconstruction efficiency, therefore, it is not expected to reproduce CLEO fit-result histograms exactly.

#### 4. Implementation of the amplitude-analysis formalism

The calculations are performed by the VECAMPFIT fitter in the following way. The main likelihood formula given by Eq. (18) is modified to use event vectors:

$$\mathcal{F} = \sum_{i_1=0}^{\lfloor \frac{N_{\text{data}}-1}{L} \rfloor} \sum_{i_2=1}^L \mathcal{L}_{i_1 i_2} + \sum_k C_k(p_{n_k}) + C(p), \quad (39)$$

where  $\lfloor \cdot \rfloor$  is the floor function,  $L$  is the vector length, and  $\mathcal{L}_{i_1 i_2}$  is the likelihood for the data event with the indices  $i_1$  and  $i_2$  given by

$$\mathcal{L}_{i_1 i_2} = \begin{cases} -2w_{i_1 i_2} \ln \left[ f_S \frac{S(\Phi_{i_1 i_2}, p_S)}{I_S} + \sum_k f_B^{(k)} \frac{B^{(k)}(\Phi_{i_1 i_2}, p_B)}{I_{B^{(k)}}} \right] & \text{if } i_1 L + i_2 \leq N_{\text{data}}, \\ 0 & \text{if } i_1 L + i_2 > N_{\text{data}}. \end{cases} \quad (40)$$

The normalization integrals  $I_S$  and  $I_B$  are given by

$$I_S = \sum_{j_1=0}^{\lfloor \frac{N_{\text{MC}}-1}{L} \rfloor} \sum_{j_2=1}^L w_{j_1 j_2} S(\Phi_{j_1 j_2}, p_S), \quad (41)$$

and

$$I_{B^{(k)}} = \sum_{j_1=0}^{\lfloor \frac{N_{\text{MC}}-1}{L} \rfloor} \sum_{j_2=1}^L w_{j_1 j_2} B^{(k)}(\Phi_{j_1 j_2}, p_B), \quad (42)$$

where the signal and background densities are set to 0 if  $j_1 L + j_2 > N_{\text{MC}}$ .

In the case of scalar calculations, the likelihoods  $\mathcal{L}_{i_1 i_2}$  in Eq. (40) are calculated for each event and then their values are summed. The VECAMPFIT library instead calculates their values for the entire vector at once using vectorized signal and background density functions. The likelihood vectors are given by

$$\vec{\mathcal{L}}_{i_1} = -2w_{i_1 i_2} \ln \left[ f_S \frac{\vec{S}(\vec{\Phi}_{i_1}, p_S)}{I_S} + \sum_k f_B^{(k)} \frac{\vec{B}^{(k)}(\vec{\Phi}_{i_1}, p_B)}{I_{B^{(k)}}} \right], \quad (43)$$

Thus, the computations require user-defined vectorized signal and background density functions  $\vec{S}$  and  $\vec{B}$  which take an event vector  $\vec{\Phi}$  as an argument. Both density functions and event vector have a fixed vector length  $L$ . The calculation of MC normalization sums  $I_S$  and  $I_{B^{(k)}}$  is vectorized in a similar way.

Vectorized VECAMPFIT subprograms and the fitter code are compiled for several fixed vector lengths. The default list of vector lengths includes  $L = 1, 2, 4, 8, 16, 32, 64$ ; it can be modified when configuring the library build if necessary. Similarly, vectorized VECAMPFIT Fortran modules are provided in several versions corresponding to a specific vector length, e.g.

VECAMPFIT\_HIGH\_ENERGY\_PHYSICS\_VECTOR\_#LENGTH# with #LENGTH# expanding into one of the lengths from the list. The modules provide generic interfaces for their subprograms so that the names do not depend on the vector lengths. For example, the subroutine for calculation of the simple constant-width Breit-Wigner amplitude from the high-energy-physics module can be called as BREIT\_WIGNER\_CONSTANT\_WIDTH\_M regardless of the vector length.

The input data and MC events need to be stored in ROOT files in trees [28]. By default, events are assumed to be stored as event class using one tree branch. The name of the tree and event-class branch are passed as arguments to the function `vecampfit_fitter_load_data_file()`; its usage is described in Sec. 5. The default storage format can be changed by specifying a user function setting branch addresses for reading of the event from the data tree using `vecampfit_fitter_set_branch_addresses_function()`.

The  $D^0 \rightarrow K^- \pi^+ \pi^0$  event class `d0_kmpippi0_event` contains four-momenta of the final-state particles:

```
class d0_kmpippi0_event : public TObject
{
    /* All member functions are omitted. */
    float km_momentum[4];
    float pip_momentum[4];
    float pi0_momentum[4];
}
```

The event-vector arguments  $\vec{\Phi}$  are called event buffers in the VECAMPFIT library. The signal event buffers in the  $D^0 \rightarrow K^- \pi^+ \pi^0$  example contain all invariant masses, momenta of the decays of the  $D^0$  to an intermediate resonance and a third particle, and momenta of the decays of an intermediate resonance to a pair of final-state particles:

```
TYPE, BIND(C) :: SIGNAL_EVENT_BUFFER_#MODEL#
REAL(C_REAL_KIND) M_KM_PIP(VECTOR_LENGTH)
REAL(C_REAL_KIND) M_KM_PIZ(VECTOR_LENGTH)
REAL(C_REAL_KIND) M_PIP_PIZ(VECTOR_LENGTH)
REAL(C_REAL_KIND) Q_DO_RHOP_KM(VECTOR_LENGTH)
REAL(C_REAL_KIND) Q_DO_KSTM_PIP(VECTOR_LENGTH)
REAL(C_REAL_KIND) Q_DO_KSTZ_PIZ(VECTOR_LENGTH)
REAL(C_REAL_KIND) Q_RHOP_PIP_PIZ(VECTOR_LENGTH)
REAL(C_REAL_KIND) Q_KSTM_KM_PIZ(VECTOR_LENGTH)
REAL(C_REAL_KIND) Q_KSTZ_KM_PIP(VECTOR_LENGTH)
END TYPE
```

Here, `C_REAL_KIND` is a C-interoperable real kind (`C_FLOAT` or `C_DOUBLE`) and `VECTOR_LENGTH` is the vector length, which are chosen during configuration. The C-interface header is generated automatically by the program `vecampfit-fortran`. The suffix `#MODEL#` is the template part and it always

has the value `DZ_KMPIPIZ_DEFAULT` for the  $D^0 \rightarrow K^-\pi^+\pi^0$  example. The templates are described in detail in Sec. 7.4. To achieve optimal performance, the event buffers should contain all data required for calculation of the signal or background density that depend on the event but not fit parameters and require complicated calculations.

The event buffers are filled once at the beginning of the fitting upon data loading by a user-defined event-buffer-filling function:

```
void fill_signal_event_buffer_#model#(void *buf, const void *ev, int index)
{
    signal_event_buffer_#model# *buffer =
        (signal_event_buffer_#model#) buf;
    const d0_kmpippi0_event *event = (const d0_kmpippi0_event*) ev;
    buffer->m_km_pip[index] = event->get_mass_km_pip();
    buffer->m_km_piz[index] = event->get_mass_km_pi0();
    /* The remaining code is omitted. */
}
```

In addition to the event buffer, the density functions also take a parameter buffer as an argument. The parameter buffer is a user-provided derived type that is used to store values depending on the fit parameters only. The signal parameter buffer in the  $D^0 \rightarrow K^-\pi^+\pi^0$  example contains buffers for individual resonances and nonresonant amplitude:

```
TYPE, BIND(C) :: SIGNAL_PARAMETER_BUFFER_#MODEL#
    TYPE(SIGNAL_PARAMETER_BUFFER_AMPLITUDE_#MODEL#) A_DO_NR
    TYPE(SIGNAL_PARAMETER_BUFFER_RESONANCE_#MODEL#) RH0770P
    ! Other resonances are omitted.
END TYPE
```

The buffers for individual resonances contain their complex amplitudes,  $m_0^{-2}$ ,  $m_0^{-3}$ , inverse momenta and formfactors at the resonance mass and their derivatives:

```
TYPE, BIND(C) :: SIGNAL_PARAMETER_BUFFER_RESONANCE_#MODEL#
    TYPE(SIGNAL_PARAMETER_BUFFER_AMPLITUDE_#MODEL#) AMP_D_R
    REAL(C_REAL_KIND) INVERSE_M2
    REAL(C_REAL_KIND) INVERSE_M3
    REAL(C_REAL_KIND) INVERSE_Q0
    REAL(C_REAL_KIND) DINVERSE_Q0_DMO
    REAL(C_REAL_KIND) INVERSE_F0
    REAL(C_REAL_KIND) DINVERSE_F0_DMO
    REAL(C_REAL_KIND) INVERSE_F0_D
    REAL(C_REAL_KIND) DINVERSE_F0_D_DMO
END TYPE
```

The parameter buffer is filled at the beginning of each likelihood-function call. The signal parameter buffer is filled in the  $D^0 \rightarrow K^-\pi^+\pi^0$  Dalitz analysis by the subroutine

```
SUBROUTINE FILL_SIGNAL_PARAMETER_BUFFER_#MODEL#(PAR_BUF, PAR) BIND(C)
```

```

USE, INTRINSIC :: ISO_C_BINDING
IMPLICIT NONE
TYPE(SIGNAL_PARAMETER_BUFFER_#MODEL#), INTENT(OUT) :: PAR_BUF
REAL(C_REAL_KIND), INTENT(IN) :: PAR(DZ_KMPIPIZ_SIGNAL_MODEL_PARAMETERS)
CALL FILL_SIGNAL_PARAMETER_BUFFER_AMPLITUDE(PAR_BUF%A_DO_NR, PAR(DO_NR_A), &
& PAR(DO_NR_P))
CALL FILL_SIGNAL_PARAMETER_BUFFER_RHOP(PAR_BUF%RH0770P, &
& PAR(RH0770P_PIP_PIZ_A), PAR(RH0770P_PIP_PIZ_P), PAR(RH0770P_MASS), &
& PAR(RH0770P_R), PAR(DO_R), 1)
! Calls for other resonances are omitted.
END SUBROUTINE

```

Actual filling is performed by individual-resonance subroutines, for example

```

SUBROUTINE FILL_SIGNAL_PARAMETER_BUFFER_AMPLITUDE(PAR_BUF, AMP_D_R_ABS, &
& AMP_D_R_ARG)
USE VECAMPFIT_MATHEMATICAL_CONSTANTS
IMPLICIT NONE
TYPE(SIGNAL_PARAMETER_BUFFER_AMPLITUDE_#MODEL#), INTENT(OUT) :: PAR_BUF
REAL(REAL_KIND), INTENT(IN) :: AMP_D_R_ABS, AMP_D_R_ARG
REAL(REAL_KIND), PARAMETER :: DEG_TO_RAD = &
& REAL(DEGREE_IN_RADIANS_REAL64, REAL_KIND)
PAR_BUF%DAMP_DABSA = EXP(CMPLX(0, AMP_D_R_ARG * DEG_TO_RAD, REAL_KIND))
PAR_BUF%AMP = AMP_D_R_ABS * PAR_BUF%DAMP_DABSA
PAR_BUF%DAMP_DARGA = CMPLX(0, DEG_TO_RAD, REAL_KIND) * PAR_BUF%AMP
END SUBROUTINE

```

The density-function subroutines have three input arguments: the event buffer, fit parameters, and parameter buffer. They have one output argument, the density vector. The density-function abstract interface is defined as

```

ABSTRACT INTERFACE
SUBROUTINE VECAMPFIT_FITTER_DENSITY_FUNCTION(DENSITY, EVENT_BUFFER, &
& PARAMETERS, PARAMETER_BUFFER) BIND(C)
USE, INTRINSIC :: ISO_C_BINDING
IMPLICIT NONE
REAL(__KIND), INTENT(OUT) :: DENSITY(__LENGTH)
INTEGER(C_INTPTR_T), INTENT(IN), VALUE :: EVENT_BUFFER
REAL(__KIND), INTENT(IN) :: PARAMETERS(*)
TYPE(C_PTR), INTENT(IN), VALUE :: PARAMETER_BUFFER
END SUBROUTINE
END INTERFACE

```

Examples of density-function implementation can be found in the files `background_density.F90` and `signal_density.F90` of the  $D^0 \rightarrow K^-\pi^+\pi^0$  example.

## 5. Fitting procedure

The  $D^0 \rightarrow K^-\pi^+\pi^0$  Dalitz analysis provides examples of basic fitting procedure in the files `d0-kmpippi0-fit-background.cc` and `d0-kmpippi0-fit-background.cc` for the signal and background, respectively. In addition,

an example of fitting-procedure control from Fortran is provided in the file `d0-kmpippi0-fit-background.F90`. The C++-based signal fit is described in detail below. The fit starts with the fitter initialization:

```

/* Alignment. */
const size_t alignment = 64;
/* Initialize fitter. */
SUBROUTINE_WITH_KIND_LENGTH(vecampfit_fitter_initialize)(
    1, DZ_KMPIPIZ_SIGNAL_PARAMETERS, "dz_kmpippiz_event",
    sizeof(dz_kmpippiz_event), alignment, false,
    options->weighted_mc || options->grid_integration,
    options->offloading);

```

The macro `SUBROUTINE_WITH_KIND_LENGTH` expands into the subroutine name followed by two suffixes denoting the variable type and kind, and vector length. The number of simultaneous-fit points is specified by the first argument. The following arguments specify the number of fit parameters, the name and size of the ROOT class which is used to store the event data, alignment of event buffers allocated by the fitter, whether the data and MC events are weighted, and whether to use GPU offloading.

Fitter initialization is followed by setting the number of background sources for each simultaneous-fit point:

```

/* Set number of background sources. */
res = vecampfit_fitter_set_n_background_sources(1, 1);
if (res != 0)
    return -1;

```

After setting the number of background sources, the sizes of the event and parameter buffers, and functions for filling of the buffers can be set:

```

/* Set function filling signal event buffer. */
res = vecampfit_fitter_set_fill_signal_event_buffer(
    fill_signal_event_buffer_#model#,
    sizeof(signal_event_buffer_#model#), 1);
if (res != 0)
    return -1;
/* Set function filling background event buffer. */
res = vecampfit_fitter_set_fill_background_event_buffer(
    fill_background_event_buffer_#model#,
    sizeof(background_event_buffer_kmpippiz_default), 1, 1);
if (res != 0)
    return -1;
/* Set function filling signal parameter buffer. */
res = vecampfit_fitter_set_fill_signal_parameter_buffer(
    VECAMPFIT_FITTER_FILL_PARAMETER_BUFFER_FUNCTION(
        fill_signal_parameter_buffer_#model#),
    sizeof(signal_parameter_buffer_#model#));
if (res != 0)
    return -1;
/* Set function filling background parameter buffer. */
res = vecampfit_fitter_set_fill_background_parameter_buffer(

```

```

VECAMPFIT_FITTER_FILL_PARAMETER_BUFFER_FUNCTION (
fill_background_parameter_buffer_kmpippiz_default),
sizeof(background_parameter_buffer_kmpippiz_default), 1, 1);
if (res != 0)
return -1;

```

The next step is setting of the signal and background density functions:

```

/* Set signal density. */
res = vecampfit_fitter_set_signal_density (
VECAMPFIT_FITTER_DENSITY_FUNCTION(signal_density_#model#), 1);
if (res != 0)
return -1;
/* Set background density. */
res = vecampfit_fitter_set_background_density (
VECAMPFIT_FITTER_DENSITY_FUNCTION (
background_density_kmpippiz_default), 1, 1);
if (res != 0)
return -1;

```

The background fractions  $f_B^{(k)}$  from Eq. (18) should be fit parameters. Their numbers are set by calling

```

/* Set background-fraction parameter. */
res = vecampfit_fitter_set_background_fraction_parameter (
BACKGROUND_FRACTION, 1, 1);
if (res != 0)
return -1;

```

If necessary, the integration type is then set. Function for filling of event class from signal parameter buffer is set for grid integration:

```

if (options->grid_integration) {
/* Set integration type to grid. */
res = vecampfit_fitter_set_normalization_integration_type (
INTEGRATION_TYPE_GRID);
if (res != 0)
return -1;
/*
* Set function filling event class from signal parameter
* buffer. It is used when writing the result ROOT file
* to fill signal events from the points of integration grid.
*/
vecampfit_fitter_set_fill_event_class (
dz_kmpippiz_fill_event_class, 1);
}

```

Random engine is initialized for assignment of initial parameters:

```

/* Set random seed for parameter initialization. */
unsigned int random_seed = options->random_seed;
if (!options->fixed_random_seed) {
res = vecampfit_urandom(&random_seed, sizeof(int));
if (res != 1)
return -1;
}
vecampfit_random_engine_set_seed(random_seed);
printf("Random seed: %u\n", random_seed);

```

The fitting then continues with loading of fit parameters:

```

/* Read signal parameters. */
std::string file_name;
if (options->generate_mc) {
    file_name = std::string(VECAMPFIT_DATA_DIRECTORY) +
        "/examples/dz_kmppiz/parameters_signal_mc.dat";
} else {
    file_name = std::string(VECAMPFIT_DATA_DIRECTORY) +
        "/examples/dz_kmppiz/parameters_signal.dat";
}
res = vecampfit_fitter_load_parameters_file(FUNCTION_TYPE_SIGNAL,
    DZ_KMPIPIZ_SIGNAL_PARAMETERS, file_name.c_str(), 1);
if (res != 0)
    return -1;
/* Read background parameters. */
file_name = std::string(VECAMPFIT_DATA_DIRECTORY) +
    "/examples/dz_kmppiz/parameters_background.dat";
res = vecampfit_fitter_load_parameters_file(FUNCTION_TYPE_BACKGROUND,
    DZ_KMPIPIZ_BACKGROUND_MODEL_PARAMETERS,
    file_name.c_str(), 1);
if (res != 0)
    return -1;

```

The parameters are stored in a text file with a single line corresponding to each parameter and containing the parameter name, its initial value  $I$ , initial numeric-minimization step, lower and upper bounds, and random change  $R$ . As in MINUIT which is used as the fitting engine, if both the lower and upper bounds are equal to zero, then the parameter is not constrained. When fitting, the initial value is chosen at random with a uniform distribution in the range  $(I - R, I + R)$ . The initial lines of the parameter file `parameters_signal.dat` for the signal fit in the  $D^0 \rightarrow K^- \pi^+ \pi^0$  example are:

```

D_R          5.0 1E-3 0E0 0E0      0E0
RHOP1_M      0.770 1E-3 0E0 0E0      0E0
RHOP1_G      0.1507 1E-3 0E0 0E0      0E0
RHOP1_R      1.5 1E-3 0E0 0E0      0E0

```

Resonance masses and widths from CLEO analysis are used.

The fit preparation finishes by reading the normalization Monte Carlo and data events:

```

/* Read normalization Monte Carlo. */
if (!(options->generate_mc && options->normalization_mc &&
    !options->weighted_mc_full_density) &&
    !options->grid_integration) {
    if (options->weighted_mc) {
        res = vecampfit_fitter_load_data_file(
            "mc_signal_weighted.root", "tree", "event",
            DATA_TYPE_MONTE_CARLO, 1, 0);
    } else {
        res = vecampfit_fitter_load_data_file("mc_signal.root",
            "tree", "event", DATA_TYPE_MONTE_CARLO, 1, 0);
    }
}

```

```

    }
    if (res != 0)
        return -1;
}
/* Read data. */
if (options->pseudoexperiment >= 0) {
    file_name = std::string("data_signal_") +
        std::to_string(options->pseudoexperiment) + ".root";
} else {
    file_name = "data_signal.root";
}
res = vecampfit_fitter_load_data_file(file_name.c_str(), "tree",
    "event", DATA_TYPE_DATA, 1, 0);
if (res != 0)
    return -1;

```

The example provides a way to choose between Monte Carlo samples with uniform distribution and weighted in accordance with the full density function.

The fitting is performed by the TMinuit class from ROOT via VECAMPFIT interface. The fitting-command sequence is

```

/* Fix all parameters. */
vecampfit_minuit_interface_fix_range(1, SIGNAL_PARAMETERS);
/* Release absolute values of the amplitudes. */
vecampfit_minuit_interface_release(DO_NR_A);
//vecampfit_minuit_interface_release(RH0770P_PIP_PIZ_A);
vecampfit_minuit_interface_release(RH01700P_PIP_PIZ_A);
vecampfit_minuit_interface_release(KST892M_KM_PIZ_A);
vecampfit_minuit_interface_release(KST01430M_KM_PIZ_A);
vecampfit_minuit_interface_release(KST1680M_KM_PIZ_A);
vecampfit_minuit_interface_release(KST892Z_KM_PIP_A);
vecampfit_minuit_interface_release(KST01430Z_KM_PIP_A);
vecampfit_minuit_interface_migrad(100000);
/* Release phases of the amplitudes. */
vecampfit_minuit_interface_release(DO_NR_P);
//vecampfit_minuit_interface_release(RH0770P_PIP_PIZ_P);
vecampfit_minuit_interface_release(RH01700P_PIP_PIZ_P);
vecampfit_minuit_interface_release(KST892M_KM_PIZ_P);
vecampfit_minuit_interface_release(KST01430M_KM_PIZ_P);
vecampfit_minuit_interface_release(KST1680M_KM_PIZ_P);
vecampfit_minuit_interface_release(KST892Z_KM_PIP_P);
vecampfit_minuit_interface_release(KST01430Z_KM_PIP_P);
/* Release background fraction. */
vecampfit_minuit_interface_release(BACKGROUND_FRACTION);
vecampfit_minuit_interface_migrad(100000);
/* Releasing of resonance masses and widths is omitted. */

```

Finally, the fit results are recorded to a ROOT file with density-function values, contributions of each background source, and original events; a parameter file suitable for another run of the fitting program; a ROOT file with the resulting minimum value of the likelihood function  $\mathcal{F}$ , parameters, errors, and error matrix with its eigenvectors and eigenvalues; and a text file with

the same results except the error matrix.

```

if (options->save_density) {
    vecampfit_fitter_write_density_root("signal_density.root", 1,
        false, options->disable_normalization);
}
vecampfit_fitter_write_result_parameters(
    "parameters_signal_result.dat");
if (options->pseudoexperiment >= 0) {
    file_name = std::string("signal_result_") +
        std::to_string(options->pseudoexperiment) + ".root";
} else {
    file_name = "signal_result.root";
}
vecampfit_write_fit_result_root(file_name.c_str());
vecampfit_fitter_write_result_text("results.txt");
if (options->offloading) {
    vecampfit_offloading_free(signal_density_device);
    vecampfit_offloading_free(signal_density_gradient_device);
}

```

Various advanced aspects of the fitting procedure are described together with  $e^+e^- \rightarrow K\bar{K}\pi\pi$  analysis workflow in Sec. 7.

## 6. VECAMPFIT subprogram overview

### 6.1. Auxiliary library parts

VECAMPFIT Fortran processing tool `vecampfit-fortran` performs parsing and syntax analysis of a subset of the Fortran 2018 standard used by the library. It is used during building to generate interface parts of Fortran subprograms implemented in submodules for their inclusion into modules, C headers containing declarations of C-interoperable subprograms, and documentation. The Fortran subprograms are documented in the code using DOXYGEN-like syntax. It is possible to specify the scalar version of vectorized subprograms and C interface if the subprogram has them. The documentation is generated in LaTeX format and compiled into PDF file during building.

The library `vecampfit-real` contains operations on real-number representation implemented in the modules `VECAMPFIT_REAL_NUMBER_VECTOR_#LENGTH#` and `VECAMPFIT_REAL_NUMBER_BASE`. They include determination of the real-number type (finite, infinity, or NaN), extraction and setting of the mantissa, exponent, or sign bit, scaling by a power of two by changing the exponent. The library also includes vectorized subprograms for conversion between integer and real numbers from the module `VECAMPFIT_TYPE_CONVERSION_VECTOR_#LENGTH#` and transfer subprograms for getting of low

and high parts of the types `INT(INT64)` and `REAL(REAL128)` implemented in the module `VECAMPFIT_TRANSFER`.

Arbitrary-precision real-number calculations implemented in `vecampfit-arbitrary-precision` are mostly written in C, the interface being provided by the module `VECAMPFIT_APR`. The arithmetic operations: addition, subtraction, multiplication, and division are implemented with guaranteed precision and rounding. Rounding modes to the nearest number, to zero, away from zero, to larger values, and to smaller values are supported. Only precisions proportional to 64 bits are currently supported. The code is validated by comparing the calculation results for random input values with the GNU MPFR library [31]. No difference is found. Performance of addition and subtraction is similar, but performance of multiplication and subtraction is much worse since short multiplication and division algorithms used in MPFR [32] are not implemented in `VECAMPFIT`. Error, exponential, logarithm, and power functions are implemented using the arbitrary-precision arithmetic without guaranteed precision. Due to its limitations, `VECAMPFIT` arbitrary-precision subsystem is currently not recommended to be used as a general-purpose arbitrary-precision library, however, it is sufficient for the needs of `VECAMPFIT` itself. The arbitrary-precision arithmetic operations and functions are used for calculation of mathematical constants described in Sec. 6.3 and series coefficients for vectorized calculation of the logarithm and exponential functions. Additionally, the arbitrary-precision calculations are used for calculation of integration points and their weights for Gauss-Legendre quadrature using the Newton's method with the starting values from Ref. [33].

## 6.2. Complex-vector type

The usual `COMPLEX` type is not well suited for vectorization, because the real and imaginary parts of complex-array elements are stored in adjacent memory regions for each array element. In order to get a vector of real or imaginary parts, it is necessary to perform permutations of the data stored in memory. Thus, a new type for complex vectors with real and imaginary parts stored in separate arrays is introduced in modules `VECAMPFIT_COMPLEX_VECTOR_#LENGTH#`:

```

TYPE TYPE_WITH_KIND_LENGTH(COMPLEX_VECTOR)
  !> Real parts.
  REAL(__KIND) RE(__LENGTH)
  !> Imaginary parts.
  REAL(__KIND) IM(__LENGTH)
END TYPE

```

This type is used for calculations involving complex amplitudes, for example, to store the results of the vectorized calculation of the Breit-Wigner amplitudes. The complex-vector modules provide vectorized subprograms for calculations with complex vectors including addition, subtraction, and multiplication of a complex vector and another complex vector, real array, real variable, or complex variable; assignment of a real or complex array or constant, negation, inversion ( $1/x$ ), conjugation, absolute value, and physical-sheet or unphysical-sheet square root. Non-vectorized subprograms include getting and setting of individual elements and sum of vector elements.

### 6.3. Mathematical subprograms

The module `VECAMPFIT_MATHEMATICAL_CONSTANTS` provides several mathematical constants in three precisions: `REAL32`, `REAL64`, and `REAL128`. The constants are calculated by the library itself during building using its arbitrary-precision operations. The list of constants currently includes  $\sqrt{2}$ ,  $\ln 2$ ,  $e$ ,  $\pi$ ,  $\sqrt{\pi/2}$ ,  $\sqrt{\pi}$ ,  $\sqrt{2\pi}$ , and coefficients for conversion between degrees and radians.

The modules `VECAMPFIT_MATHEMATICAL_FUNCTIONS_VECTOR_#LENGTH#` contain implementations of general mathematical functions and the module `VECAMPFIT_MATHEMATICAL_FUNCTIONS` implements their scalar versions. Similarly, other vectorized modules described below have the corresponding scalar versions. The mathematical functions include vectorized versions of exponential, floor, logarithm, and power functions, calculation of the Gaussian function, asymmetric Gaussian function, asymmetric Gaussian functions with various non-Gaussian tails (exponential, exponential and power-law, power-law, and power-law transiting to exponential ones), Chebyshev polynomials [34], Källén lambda function [35], and logistic function.

The modules `VECAMPFIT_GEOMETRY_VECTOR_#LENGTH#` contain a function for determination of the difference between two azimuthal angles in the range  $[-\pi, \pi)$ . Linear interpolation is implemented in the modules `VECAMPFIT_INTERPOLATION_VECTOR_#LENGTH#`. The modules `VECAMPFIT_LINEAR_ALGEBRA_VECTOR_#LENGTH#` contain  $LU$  decomposition and calculation of determinant of a vector of  $2 \times 2$  complex matrices. The corresponding scalar module includes conversion between compact and full forms of a symmetric matrix and calculation of a symmetric-matrix eigenvectors and eigenvalues performed using LAPACK [36]. The module `VECAMPFIT_NUMERIC_INTEGRATION` implements one-dimensional Simpson integration, adaptive multidimensional Genz-Malik integration [37], and a subroutine getting Gauss-Legendre quadrature data: integration points and their weights.

Statistical functions are included into two modules: generalization of Feldman-Cousins confidence intervals [38] to asymmetric-Gaussian likelihood is implemented in the module `VECAMPFIT_STATISTICS`, and the module `VECAMPFIT_MIXED_SAMPLE` contains subroutines for the mixed-sample method [39, 40].

#### 6.4. Physical subprograms

Kinematic subprograms are implemented in the modules `VECAMPFIT_KINEMATICS_VECTOR_#LENGTH#` and include covariant factor given by Eq. (78) (subroutine `COVARIANT_FACTOR`), momentum of a daughter particle in the mother rest frame for the decay  $0 \rightarrow 1 + 2$  (subroutine `DECAY_MOMENTUM`) given by

$$q = \frac{\sqrt{(m_0^2 - (m_1 + m_2)^2)(m_0^2 - (m_1 - m_2)^2)}}{2m_0}, \quad (44)$$

and closely-related two-body phase-space factor (`PHASE_SPACE_2BODY_COMPLEX`) given by

$$\rho = \frac{1}{16\pi} \frac{\sqrt{(s - (m_1 + m_2)^2)(s - (m_1 - m_2)^2)}}{s}, \quad (45)$$

where the Mandelstam variable  $s$  is complex as this function is intended to be used for determination of  $T$ -matrix poles. The scalar module `VECAMPFIT_KINEMATICS` also has functions for conversion of helicity-formalism variables into four-momenta and Dalitz-plot subprograms: determination of cosine of the helicity angle, range of the squared invariant mass  $m_{23}^2$  depending on the squared invariant mass  $m_{12}^2$ , and checking whether the squared invariant masses  $m_{12}^2$  and  $m_{23}^2$  are into the allowed kinematic region of the Dalitz plot. Three and four-dimensional vectors are implemented in the modules `VECAMPFIT_VECTOR3` and `VECAMPFIT_VECTOR4`.

The modules `VECAMPFIT_HIGH_ENERGY_PHYSICS_VECTOR_#LENGTH#` contain high-energy-physics subprograms including the Blatt-Weisskopf formfactors, various forms of the Breit-Wigner amplitude, covariant factors given by Eq. (79) (subroutines `COVARIANT_FACTOR*`), and  $K$ -matrix amplitude parameterization [41]. The Blatt-Weisskopf formfactors [30] are given by Eq. (35); squared formfactors and their ratios (subroutines `BLATT_WEISSKOPF*`) are included into the library.

The Breit-Wigner amplitudes include the amplitude with known daughter momenta and formfactors with a phase-space factor given by Eq. (57) (subroutines `BREIT_WIGNER_Q_F*`) and without the phase-space factor given by Eq. (34) (subroutines `BREIT_WIGNER_Q_F_NOPHSP*`). The Breit-Wigner

amplitude with a constant width (subroutines BREIT\_WIGNER\_CONSTANT\_WIDTH\*) is given by

$$B(m) = \frac{1}{m_0^2 - m^2 - im\Gamma_0} \quad (46)$$

or

$$B(m) = \frac{1}{m_0^2 - m^2 - im_0\Gamma_0}. \quad (47)$$

The general form of the Breit-Wigner amplitude (subroutine BREIT\_WIGNER\_GENERAL) is given by

$$B(m) = \frac{\mathcal{N}(m)}{m_0^2 - m^2 - i\mathcal{G}(m)}, \quad (48)$$

where  $m_0$  is the resonance mass,  $m = \sqrt{s}$  is the invariant mass,  $\mathcal{N}(m) = \alpha g_a n_a(m)$  is the product of coupling and formfactor coupling for the current decay channel, and  $\mathcal{G}(m) = m_0\Gamma(m) = \sum_b g_b^2 \rho_b(m) n_b^2(m)$  is the sum of products of squared formfactor, phase-space factor, and squared coupling for all channels [42]. The Breit-Wigner matrix element (subroutine BREIT\_WIGNER\_M2) is given by

$$B(m) = \frac{\left(\frac{q}{q_0}\right)^{2L+1} \frac{F_L^2(q)}{F_L^2(q_0)}}{(m_0^2 - m^2)^2 + m_0^2\Gamma^2(m)}. \quad (49)$$

Another group of high-energy-physics subprograms is related to  $K$ -matrix amplitude [41]. The  $K$ -matrix is given by

$$K_{\alpha\beta} = b_{\alpha\beta} + \sum_R \frac{g_\alpha g_\beta}{m_R^2 - s}, \quad (50)$$

where  $b$  is the nonresonant part,  $g$  are resonance couplings, and  $m_R$  are their bare masses. The  $P$ -vector describing the production amplitude with the appropriate pole structure is given by

$$P_\alpha = a_\alpha + \sum_R A_R \frac{g_\alpha}{m_R^2 - s}, \quad (51)$$

where  $a$  is the nonresonant production amplitude and  $A_R$  is resonance production amplitude. Subroutines for addition of poles to both  $K$ -matrix and  $P$ -vector are available for one- and two-channel  $K$ -matrices.

The  $K$ -matrix amplitude is given by

$$A = n[I - iK\rho n^2]^{-1}P, \quad (52)$$

where  $I$  is identity matrix,  $\rho$  is diagonal matrix with elements equal to phase-space factor given by Eq. (45), and  $n$  is a diagonal kinematic-factor matrix containing the centrifugal barrier near threshold and formfactor, which is calculated as

$$n_k = \left(\frac{q}{q_0}\right)^L \frac{F(q)}{F(q_0)}, \quad (53)$$

where  $k$  is channel number,  $q$  is decay momentum,  $q_0$  is momentum scale,  $L$  is the angular momentum, and  $F$  is a formfactor. Subroutines for calculation of the matrix  $I - iK\rho n^2$  and their version for  $S$  wave without  $n^2$  are available for one- and two-channel  $K$ -matrices.

Momentum analytic continuation (subroutine `MOMENTUM_ANALYTIC_CONTINUATION`) is given by

$$q_{\text{cont}} = \begin{cases} q & \text{for } m_0 \geq m_1 + m_2, \\ i\sqrt{-|q|^2} & \text{for } m_0 < m_1 + m_2, \end{cases} \quad (54)$$

where  $|q|^2$  is calculated as in Eq. (44) with both its sides squared. The same analytic continuation is used in the Flatté distribution [43].

Quantum-mechanics subprograms are implemented in the module `VECAMPFIT_QUANTUM_MECHANICS`. Wigner  $d$  functions [44] (function `D_FUNCTION`) are given by

$$\begin{aligned} d_{m_1 m_2}^J(\theta) &= \sqrt{(j+m_1)!(j-m_1)!(j+m_2)!(j-m_2)!} \\ &\times \sum_{k=\max(0, m-m_2)}^{\min(j+m_1, j-m_2)} \frac{(-1)^k (\cos \frac{\theta}{2})^{2j+m_2-m_1-2k} (-\sin \frac{\theta}{2})^{m_1-m_2+2k}}{(j-m_1-k)!(j+m_2-k)!(k+m_1-m_2)!k!}. \end{aligned} \quad (55)$$

The subroutine `ANGULAR_MOMENTUM_RANGE` returns minimum and maximum angular momentum allowed in a two-body decay taking into account spin and parity of all particles and whether the parity is conserved.

### 6.5. Other data-analysis functions

The module `VECAMPFIT_GENERATION` implements subroutines for generation of Monte Carlo for two-body and multi-body decays with uniform phase-space distribution. The algorithm for generation of multi-body decays is described in [45].

It is necessary to know the masses of the initial and final-state particles for calculation of the amplitudes. The masses of weakly-decaying and narrow states are provided as constants in VECAMPFIT, while the parameters of the intermediate resonances are supposed to be represented by the fit parameters. Parameter variables PDG\_2020, PDG\_2022, and PDG\_2024 are defined in the module VECAMPFIT\_PARTICLE\_DATA, containing the 2020 [46], 2022 [47], and 2024 [42] Particle Data Group data, respectively.

The fitter is written in Fortran but the data are stored using ROOT C++ libraries. VECAMPFIT has several ROOT interface modules providing Fortran interfaces for the classes TMinuit, TFile, TRandom1, and TTree. A small part of VECAMPFIT is written for usage with ROOT, including calculation of helicity and azimuthal angles using ROOT Lorentz vectors and data object for storage of value with errors.

## 7. Analysis workflow example

The process  $e^+e^- \rightarrow K^+K^-\pi^+\pi^-$  has been studied by BABAR [48], CMD-3 [49] and BESIII [50]. The CMD-3 collaboration performed an amplitude fit, however, it was not a full amplitude analysis because of additional restrictions on relative phases of various amplitudes, which were only allowed to be equal to 0 or  $\pi$ . It was found that the dominant contributions to the amplitude are  $e^+e^- \rightarrow K_1(1270)^+K^-$  and  $e^+e^- \rightarrow K_1(1400)^+K^-$ . The fit has been performed at 9 combined energy points with  $\sqrt{s}$  from 1600 to 2000 MeV. One-dimensional studies by BABAR also indicate the presence of the  $K_1(1270)^+$  and  $K_1(1400)^+$  resonances. The process  $e^+e^- \rightarrow K_S^0K_S^0\pi^+\pi^-$  has been studied by BABAR [51] and CMD-3 [52].

A simplified simultaneous amplitude analysis of the processes  $e^+e^- \rightarrow K^+K^-\pi^+\pi^-$  and  $e^+e^- \rightarrow K_S^0K_S^0\pi^+\pi^-$  is implemented as an example of analysis workflow. It includes parameterizations of efficiency, resolution, background, and fit to the signal events. The fit is performed at 5 different energy points with  $\sqrt{s} = 1800, 1850, 1900, 1950, \text{ and } 2000$  MeV simultaneously.

### 7.1. Formalism

The decay chains are similar for both  $e^+e^- \rightarrow K^+K^-\pi^+\pi^-$  and  $e^+e^- \rightarrow K_S^0K_S^0\pi^+\pi^-$ . The final-state particles are denoted as  $e^+e^- \rightarrow K^{(1)}\bar{K}^{(2)}\pi^{(1)}\pi^{(2)}$ . There are four chains proceeding via three-body resonances:  $\gamma^* \rightarrow K_J^{(1)}\bar{K}^{(2)}$ ,  $K_J^{(1)} \rightarrow K^{(1)}\pi^{(1)}\pi^{(2)}$ ;  $\gamma^* \rightarrow \bar{K}_J^{(2)}K^{(1)}$ ,  $\bar{K}_J^{(2)} \rightarrow \bar{K}^{(2)}\pi^{(2)}\pi^{(1)}$ ;  $\gamma^* \rightarrow a_J^{(1)}\pi^{(2)}$ ,  $a_J^{(1)} \rightarrow \pi^{(1)}K^{(1)}\bar{K}^{(2)}$ ;  $\gamma^* \rightarrow a_J^{(2)}\pi^{(1)}$ ,  $a_J^{(2)} \rightarrow \pi^{(2)}\bar{K}^{(2)}K^{(1)}$ . The three-body

state has three possible decay channels; for example, for the first chain they are  $K_J^{(1)} \rightarrow K_J^{*(11)}\pi^{(2)}$ ,  $K_J^{*(11)} \rightarrow K^{(1)}\pi^{(1)}$  (cannot proceed through conventional resonances for  $e^+e^- \rightarrow K^+K^-\pi^+\pi^-$ );  $K_J^{(1)} \rightarrow K_J^{*(12)}\pi^{(1)}$ ,  $K_J^{*(12)} \rightarrow K^{(1)}\pi^{(2)}$ ;  $K_J^{(1)} \rightarrow \rho_J K^{(1)}$ ,  $\rho_J \rightarrow \pi^{(1)}\pi^{(2)}$ . In addition, there are three decay chains with a pair of two-body resonances:  $\gamma^* \rightarrow \phi_J f_J$ ,  $\phi_J \rightarrow K^{(1)}\bar{K}^{(2)}$ ,  $f_J \rightarrow \pi^{(1)}\pi^{(2)}$ ;  $\gamma^* \rightarrow K_J^{*(11)}\bar{K}_J^{*(22)}$ ,  $K_J^{*(11)} \rightarrow K^{(1)}\pi^{(1)}$ ,  $\bar{K}_J^{*(22)} \rightarrow \bar{K}^{(2)}\pi^{(2)}$ ;  $\gamma^* \rightarrow K_J^{*(12)}\bar{K}_J^{*(21)}$ ,  $K_J^{*(12)} \rightarrow K^{(1)}\pi^{(2)}$ ,  $\bar{K}_J^{*(21)} \rightarrow \bar{K}^{(2)}\pi^{(1)}$ .

The decay phase space is 7-dimensional. It is convenient to use the  $\gamma^* \rightarrow \phi_J f_J$  decay chain for resolution determination because narrow resonances  $\phi$  and  $\omega$  are expected to be observed in the  $K^+K^-$  and  $\pi^+\pi^-$  invariant masses, respectively. For this chain, the helicity-formalism variables are

$$\Phi = (\theta_{\gamma^*}^{(5)}, M_{K^{(1)}\bar{K}^{(2)}}, \theta_{\phi_J}^{(5)}, \varphi_{K^{(1)}}^{(5)}, M_{\pi^{(1)}\pi^{(2)}}, \theta_{f_J}^{(5)}, \varphi_{\pi^{(1)}}^{(5)}), \quad (56)$$

where  $\theta$  and  $\varphi$  are the helicity and azimuthal angles of the particle specified by the subscript, respectively, and the index in round brackets specifies the decay chain. These variables are used for parameterization of efficiency, resolution, and background.

Two-body resonances are described by the Breit-Wigner amplitude including a phase-space factor:

$$B_R(m) = \frac{\left(\frac{q}{q_0}\right)^L \frac{F_L(q)}{F_L(q_0)}}{m_0^2 - m^2 - im_0\Gamma(m)}, \quad (57)$$

where  $\Gamma(m)$  is the same as in Eq. (34). Three-body resonances are described by the Breit-Wigner amplitude with a constant width and the invariant mass in the imaginary part of the denominator:

$$B_R^{(m)}(m) = \frac{1}{m_0^2 - m^2 - im\Gamma_0}. \quad (58)$$

This is a simplification suitable for an example but not for real data analysis. In an actual analysis, it is necessary to take the dependence of the  $K_J$  decay matrix element on  $K\pi\pi$  invariant mass into account and calculate the mass-dependent width similar to Ref. [53].

The amplitude is calculated using helicity formalism (for actual analysis, covariant formalism is usually preferred for annihilation processes in this

energy range). The result is

$$\begin{aligned}
A_{\lambda_{\gamma^*}}^{\gamma^* \rightarrow K_J^{(1)} \bar{K}^{(2)}}(\Phi) = & \sum_{\lambda_{K_J^{(1)}} = -1, 0, 1} d_{\lambda_{\gamma^*} \lambda_{K_J^{(1)}}}^1(\theta_{\gamma^*}^{(1)}) \sum_{K_J^{(1)}} H_{\lambda_{K_J^{(1)}} 0}^{(\gamma^* \rightarrow K_J^{(1)} \bar{K}^{(2)})} B_{K_J^{(1)}}^{(m)}(M_{K^{(1)} \pi^{(1)} \pi^{(2)}}) \\
& \times \left( A_{\lambda_{K_J^{(1)}}}^{(K_J^{(1)} \rightarrow K_J^{*(11)} \pi^{(2)})}(\Phi) + A_{\lambda_{K_J^{(1)}}}^{(K_J^{(1)} \rightarrow K_J^{*(12)} \pi^{(1)})}(\Phi) + A_{\lambda_{K_J^{(1)}}}^{(K_J^{(1)} \rightarrow \rho_J K^{(1)})}(\Phi) \right), \tag{59}
\end{aligned}$$

where  $\lambda$  is the helicity of the particle specified by the subscript,  $d$  are Wigner  $d$  functions [44],  $H$  are helicity amplitudes,

$$\begin{aligned}
A_{\lambda_{K_J^{(1)}}}^{(K_J^{(1)} \rightarrow K_J^{*(11)} \pi^{(2)})}(\Phi) = & e^{i\lambda_{K_J^{(1)}} \varphi_{K_J^{*(11)}}^{[1]}} \sum_{\lambda_{K_J^{*(11)}} = -J(K_J^{(1)})}^{J(K_J^{(1)})} d_{\lambda_{K_J^{(1)}} \lambda_{K_J^{*(11)}}}^{J(K_J^{(1)})}(\theta_{K_J^{(1)}}^{[1]}) \\
& \times \sum_{J(K_J^{*(11)})} e^{i\lambda_{K_J^{*(11)}} \varphi_{K^{(1)}}^{[1]}} d_{\lambda_{K_J^{*(11)}} 0}^{J(K_J^{*(11)})}(\theta_{K_J^{*(11)}}^{[1]}) \\
& \times \sum_{K_J^{*(11)}} H_{\lambda_{K_J^{*(11)}} 0}^{(K_J^{(1)} \rightarrow K_J^{*(11)} K^{(1)})} H_{00}^{(K_J^{*(11)} \rightarrow K^{(1)} \pi^{(1)})} B_{K_J^{*(11)}}(M_{K^{(1)} \pi^{(1)}}), \tag{60}
\end{aligned}$$

$$\begin{aligned}
A_{\lambda_{K_J^{(1)}}}^{(K_J^{(1)} \rightarrow K_J^{*(12)} \pi^{(1)})}(\Phi) = & e^{i\lambda_{K_J^{(1)}} \varphi_{K_J^{*(12)}}^{[2]}} \sum_{\lambda_{K_J^{*(12)}} = -J(K_J^{(1)})}^{J(K_J^{(1)})} d_{\lambda_{K_J^{(1)}} \lambda_{K_J^{*(12)}}}^{J(K_J^{(1)})}(\theta_{K_J^{(1)}}^{[2]}) \\
& \times \sum_{J(K_J^{*(12)})} e^{i\lambda_{K_J^{*(12)}} \varphi_{K^{(1)}}^{[2]}} d_{\lambda_{K_J^{*(12)}} 0}^{J(K_J^{*(12)})}(\theta_{K_J^{*(12)}}^{[2]}) \\
& \times \sum_{K_J^{*(12)}} H_{\lambda_{K_J^{*(12)}} 0}^{(K_J^{(1)} \rightarrow K_J^{*(12)} K^{(1)})} H_{00}^{(K_J^{*(12)} \rightarrow K^{(1)} \pi^{(2)})} B_{K_J^{*(12)}}(M_{K^{(1)} \pi^{(2)}}), \tag{61}
\end{aligned}$$

and

$$\begin{aligned}
A_{\lambda_{K_J^{(1)}}}^{(K_J^{(1)} \rightarrow \rho_J K^{(1)})}(\Phi) &= e^{i\lambda_{K_J^{(1)}} \varphi_{\rho_J}^{[3]}} \sum_{\lambda_{\rho_J} = -J(K_J^{(1)})}^{J(K_J^{(1)})} d_{\lambda_{K_J^{(1)}} \lambda_{\rho_J}}^{J(K_J^{(1)})}(\theta_{K_J^{(1)}}^{[3]}) \\
&\times \sum_{J(\rho_J)} e^{i\lambda_{\rho_J} \varphi_{\pi^{(1)}}^{[3]}} d_{\lambda_{\rho_J} 0}^{J(\rho_J)}(\theta_{\rho_J}^{[3]}) \\
&\times \sum_{\rho_J} H_{\lambda_{\rho_J} 0}^{(K_J^{(1)} \rightarrow \rho_J K^{(1)})} H_{00}^{(\rho_J \rightarrow \pi^{(1)} \pi^{(2)})} B_{\rho_J}(M_{\pi^{(1)} \pi^{(2)}}).
\end{aligned} \tag{62}$$

The helicity amplitudes are calculated from partial-wave amplitudes, which are used as actual fit parameters, using Eq. (B5) from Ref. [54]. The partial-wave amplitudes of isospin-related channels of the decays  $K^* \rightarrow K\pi$  and  $\rho \rightarrow \pi\pi$ , as well as ratios between the partial-wave amplitudes of isospin-related channels of the decays  $K_J \rightarrow K^*\pi$  and  $K_J \rightarrow \rho K$  are fixed at the corresponding Clebsh-Gordan coefficients. For both  $e^+e^- \rightarrow K^+K^-\pi^+\pi^-$  and  $e^+e^- \rightarrow K_S^0 K_S^0 \pi^+ \pi^-$ , the second decay chain  $\gamma^* \rightarrow \bar{K}_J^{(2)} K^{(1)}$ ,  $\bar{K}_J^{(2)} \rightarrow \bar{K}^{(2)} \pi^{(2)} \pi^{(1)}$  is charge-conjugate to the first one and its amplitude  $A_{\lambda_{\gamma^*}}^{\gamma^* \rightarrow \bar{K}_J^{(2)} K^{(1)}}$  has the same partial-wave amplitudes. Only the dominant contributions  $e^+e^- \rightarrow K_1(1270)\bar{K}$  and  $e^+e^- \rightarrow K_1(1400)\bar{K}$  are included into the example, thus, implementation of other decay chains is not necessary. Decays to  $\rho(770)K^+$  and  $K^*(892)\pi^+$  are included for both  $K_1(1270)^+$  and  $K_1(1400)$ . The signal density function in case of a non-polarized beam is

$$S = \sum_{\lambda_{\gamma^*} = -1, 1} |A_{\lambda_{\gamma^*}}^{\gamma^* \rightarrow K_J^{(1)} \bar{K}^{(2)}}(\Phi) + A_{\lambda_{\gamma^*}}^{\gamma^* \rightarrow \bar{K}_J^{(2)} K^{(1)}}(\Phi)|^2. \tag{63}$$

## 7.2. Efficiency parameterization and fits with explicit gradient calculation

Parameterization of reconstruction efficiency is generally not necessary for signal fitting because the likelihood function given by Eq. (21) takes the efficiency into account via distribution of the normalization MC events passed through detector simulation. Parameterization of the efficiency is used in the  $e^+e^- \rightarrow K\bar{K}\pi\pi$  example for generation of resolution fit-result histograms. It may also be necessary to parameterize the efficiency to generate pseudoexperiments with the same distribution of signal events as in data.

The efficiency is determined by fitting a generator-level signal MC sample with information whether event was reconstructed. For real analysis, such

sample can be produced by passing generator-level events through full Geant4 detector simulation [55, 56, 57]. A simple parameterization is used in the example instead. The reconstruction efficiency is calculated as a product of efficiencies for individual final-state particles:

$$\epsilon(\Phi^{(\text{lab})}) = \prod_{K^{(1)}, \bar{K}^{(2)}, \pi^{(1)}, \pi^{(2)}} \epsilon_f(\Phi_f^{(\text{lab})}), \quad (64)$$

where  $f$  is the final-state particle index,  $\Phi_f^{(\text{lab})}$  is the laboratory-frame phase space for individual final-state particle, and  $\Phi^{(\text{lab})}$  is the laboratory-frame phase space for all final-state particles. The laboratory-frame phase-space variables are not independent due to kinematic constraints from the decay. For tracks

$$\begin{aligned} \epsilon_f(\Phi_f^{(\text{lab})}) = & 0.92[1.0 - 0.2 \exp(-5.0p_t)] \\ & \times T(\cos \theta, -0.8, 200)T(-\cos \theta, 0.8, 200)T(p_t, 0.1, 200), \end{aligned} \quad (65)$$

where  $p_t$  is the transverse momentum measured in GeV/ $c$ ,  $\theta$  is the polar angle in the laboratory frame and  $T$  is the logistic function describing thresholds:

$$T(x, x_0, k) = \frac{1}{1 + \exp[-k(x - x_0)]}. \quad (66)$$

The calibrated ratio between the efficiencies in data and MC is given by

$$R(\Phi^{(\text{lab})}) = \prod_{K^{(1)}, \bar{K}^{(2)}, \pi^{(1)}, \pi^{(2)}} R_f(\Phi_f^{(\text{lab})}), \quad (67)$$

where for tracks

$$R_f = 0.99 - 0.02 \exp(-p_t). \quad (68)$$

The efficiency is multiplied by this correction when generating data events and it is used as weight for MC events.

The efficiency parameterization used for fitting is given by

$$E(\Phi^{(\text{lab})}, \Phi) = \text{Sig} \left( \text{Sig}^{-1}(\min[\max(E_0(\Phi^{(\text{lab})}), \epsilon_1), 1 - \epsilon_1] + P_1(\Phi)), \right), \quad (69)$$

where  $\Phi$  is the decay phase space,  $\epsilon_1 = 1 \times 10^{-15}$ ,  $P_1$  is a seven-dimensional first-order polynomial, Sig is the sigmoid (standard logistic) function

$$\text{Sig}(x) = \frac{1}{1 + e^{-x}}, \quad \text{Sig}^{-1}(x) = -\ln\left(\frac{1}{x} - 1\right), \quad (70)$$

and  $E_0$  is the efficiency before correction given by

$$E_0(\Phi^{(\text{lab})}) = \prod_{K^{(1)}, \bar{K}^{(2)}, \pi^{(1)}, \pi^{(2)}} P_n(x_{p_t}, \cos \theta) T(\cos \theta, (\cos \theta)_{\min}, k_1) \\ \times T(-\cos \theta, -(\cos \theta)_{\max}, k_2) T(x_{p_t}, (x_{p_t})_{\min}, k_3), \quad (71)$$

where  $P_n$  is a two-dimensional polynomial using Chebyshev polynomials as a basis, its order  $n$  being 4 for  $e^+e^- \rightarrow K^+K^-\pi^+\pi^-$  and 8 for  $e^+e^- \rightarrow K_S^0K_S^0\pi^+\pi^-$ ,  $x_{p_t}$  is linearly transformed transverse momentum:

$$x_{p_t} = \frac{p_t}{2p_{\max}} - 1, \quad (72)$$

where  $p_{\max}$  is maximum momentum, which corresponds to the minimum invariant mass of combination of the other three particles,  $(\cos \theta)_{\min}$ ,  $(\cos \theta)_{\max}$ ,  $(x_{p_t})_{\min}$ , and  $k_i$  are threshold parameters.

An unbinned maximum likelihood fit is performed using generator-level events. The likelihood is

$$\mathcal{L}(\Phi_j^{(\text{lab})}, \Phi_j) = \begin{cases} -2 \ln g \left( \frac{E(\Phi_j^{(\text{lab})}, \Phi_j)}{w_j} \right) & \text{for reconstructed events,} \\ -2 \ln \left[ 1 - g \left( \frac{E(\Phi_j^{(\text{lab})}, \Phi_j)}{w_j} \right) \right] & \text{for non-reconstructed events,} \end{cases} \quad (73)$$

where  $j$  is the MC event index,  $w_j$  is the event weight, and

$$g(x) = \begin{cases} \epsilon_1 & \text{for } x < \epsilon_1, \\ x & \text{for } \epsilon_1 \leq x < 1 - \epsilon_2, \\ 1 - \epsilon_2 + \frac{\epsilon_2[x - (1 - \epsilon_2)]}{\epsilon_2 + [x - (1 - \epsilon_2)]} & \text{for } 1 - \epsilon_2 \leq x, \end{cases} \quad (74)$$

where  $\epsilon_2 = 1 \times 10^{-5}$ . The function  $g(x)$  protects against appearance of incorrect efficiency values during fitting. If it is necessary to determine the efficiency in data, then weights are defined as the ratio between the efficiencies in data and MC:  $w_j = R(\Phi_j) = E_{\text{data}}(\Phi_j)/E_{\text{MC}}(\Phi_j)$ . If it is necessary to determine the efficiency in MC, then  $w_j = 1$ .

Projections of efficiency fit results onto  $M_{K^{(1)}\bar{K}^{(2)}}$ ,  $M_{K^{(1)}\pi^{(2)}}$ , and  $M_{\pi^{(1)}\pi^{(2)}}$  for the energy point  $\sqrt{s} = 2000$  MeV are shown in Fig. 2.

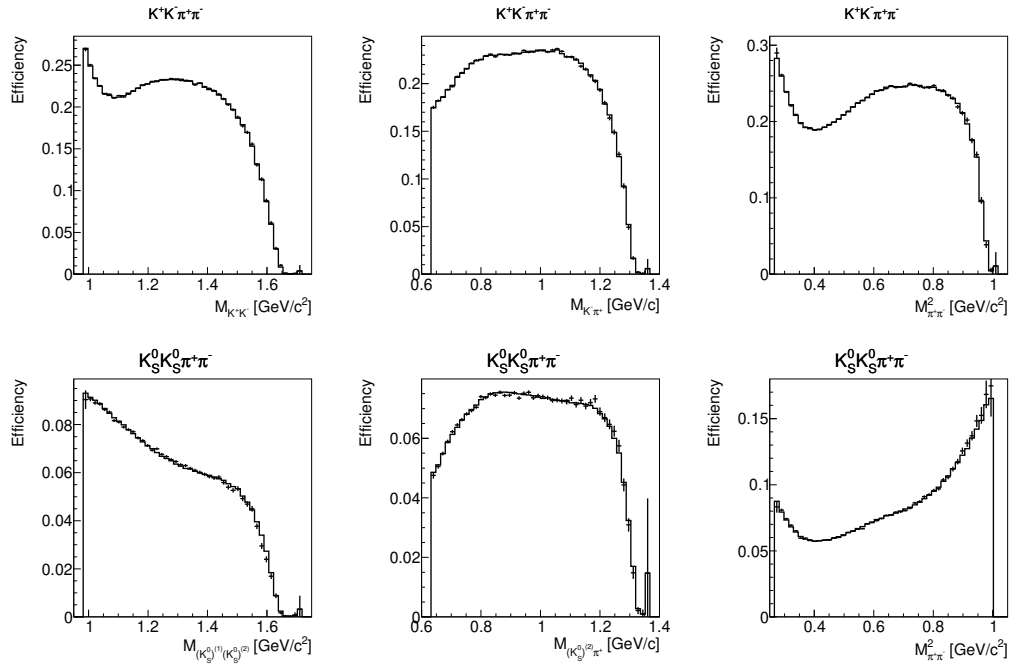


Figure 2: Projections of efficiency fit results onto  $M_{K^{(1)} \bar{K}^{(2)}}$ ,  $M_{K^{(1)} \pi^{(2)}}$ , and  $M_{\pi^{(1)} \pi^{(2)}}$  for the energy point  $\sqrt{s} = 2000$  MeV. The points with error bars are efficiency (fraction of reconstructed MC events) and the solid line is the fit result.

The efficiency fit provides an example of a fit with explicit gradient calculation. Two different signal density functions with and without gradient calculation need to be implemented, and minimization type should also be set:

```

/* Set signal density. */
res = vecampfit_fitter_set_signal_density(
    VECAMPFIT_FITTER_DENSITY_FUNCTION(
        eff_density_#model#_#process#_#sample#), 1);
if (res != 0)
    return -1;
/* Set signal density with gradient. */
res = vecampfit_fitter_set_signal_density_gradient(
    VECAMPFIT_FITTER_DENSITY_GRADIENT_FUNCTION(
        eff_density_gradient_#model#_#process#_#sample#), 1);
if (res != 0)
    return -1;
/* Use explicit gradient calculation. */
vecampfit_fitter_set_minimization_type(MINIMIZATION_GRADIENT);

```

The density function with gradient calculation has an additional output argument for gradient:

```

MODULE SUBROUTINE EFF_DENSITY_GRADIENT_#MODEL#_#PROCESS#_#SAMPLE#( &
&   ED, GRADIENT, EV, PAR, PAR_BUF) BIND(C)
  USE, INTRINSIC :: ISO_C_BINDING
  USE VECAMPFIT_REAL_VECTOR_MODULE
  IMPLICIT NONE
  REAL(C_REAL_KIND), INTENT(OUT) :: ED(VECTOR_LENGTH)
  TYPE(VECAMPFIT_T_REAL_VECTOR), INTENT(OUT) :: &
&   GRADIENT(EPEM_KKPIPI_EFFICIENCY_MODEL_PARAMETERS)
  TYPE(EEB_#MODEL#_#PROCESS#_#SAMPLE#), INTENT(IN) :: EV
  REAL(C_REAL_KIND), INTENT(IN) :: &
&   PAR(EPEM_KKPIPI_EFFICIENCY_MODEL_PARAMETERS)
  TYPE(EPB_#MODEL#_#PROCESS#_#SAMPLE#), INTENT(IN) :: PAR_BUF
  ! The calculation is omitted.
END SUBROUTINE

```

An array of real vectors defined similarly to the complex ones is used to store the gradient instead of a plain two-dimensional array for interoperability with C.

Polynomials with arbitrary coefficients are necessary for parameterizations of efficiency, resolution, and background. VECAMPFIT includes a tool `vecampfit-polynomial-parameters` for automatic generation of Fortran code for polynomials. An example can be found in the file `efficiency_correction_polynomial.F90`. The correction polynomial  $P_1(\Phi)$  from Eq. (69) is generated by calling

```

vecampfit-polynomial-parameters 2 7 --minimum-order=1 --preprocessor-order \
--subroutine

```

The code includes orders up to 2, but only the first order is actually used. Using other options, the polynomial-parameter tool can also generate the version of the same subroutine with gradient calculation, preprocessor definitions for polynomial parameters, parameter file with their initial values, and C++ code for parameter releasing.

### 7.3. Resolution parameterization and generation models

The resolution is parameterized by a 12-dimensional Gaussian function:

$$R(\Phi^{(\text{lab})}, \Phi'^{(\text{lab})}) = \frac{1}{(2\pi)^6 \sqrt{\det C}} \exp\left(-\frac{1}{2} x^T C^{-1} x\right), \quad (75)$$

where  $\Phi$  is the phase space for reconstructed kinematic parameters,  $\Phi'$  is the phase space for true (generator-level) kinematic parameters,  $C$  is covariance matrix and  $x$  is the vector of differences between true and reconstructed values:

$$x^T = (\Delta p_{K^{(1)}}/p_{K^{(1)}}, \Delta \cos \theta_{K^{(1)}}, \Delta \phi_{K^{(1)}}, \dots) \quad (76)$$

Only diagonal covariance-matrix elements are used. Each element is a first-order polynomial depending on the decay phase space  $\Phi$ . The resolution density function is normalized by construction, no numerical integration is necessary.

To represent fit results, MC events are first generated with probability density equal to the MC efficiency  $E(\Phi^{(\text{lab})}, \Phi)$  determined at the previous step. Then, a multidimensional Gaussian generator is used to generate the corresponding reconstructed values in accordance with the resolution fit result. Resolution in  $M_{K^{(1)}\bar{K}^{(2)}}$ ,  $M_{\pi^{(1)}\pi^{(2)}}$ , and  $\theta_{\phi_J}^{(5)}$  for the energy point  $\sqrt{s} = 2000$  MeV is shown in in Fig. 3.

VECFIT provides base classes for event generation: `generation_model_resolution` and `generation_model` for resolution and any other fits, respectively. The user needs to implement filling of parameter buffer:

```
/**
 * Fill parameter buffer.
 */
virtual void fill_parameter_buffer() = 0;
```

which can be done by simply calling the filling function used by the fit. For resolution fits, it is also necessary to implement generation of reconstructed event from generator-level event:

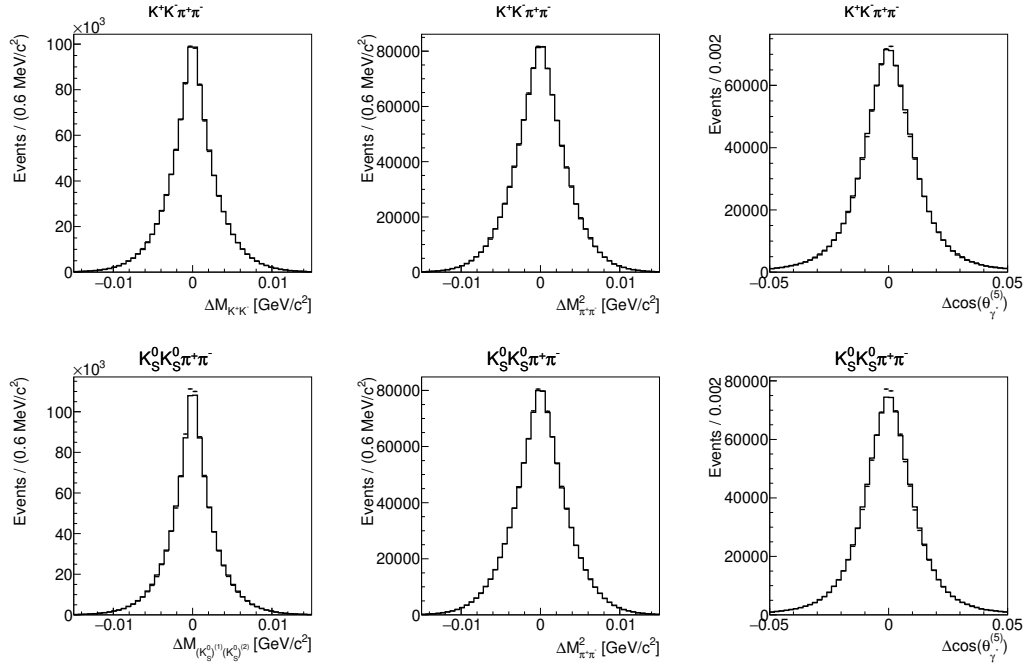


Figure 3: Resolution in  $M_{K^{(1)}\bar{K}^{(2)}}$ ,  $M_{\pi^{(1)}\pi^{(2)}}$ , and  $\theta_{\phi_J}^{(5)}$  for the energy point  $\sqrt{s} = 2000$  MeV. The points with error bars are resolution (difference between reconstructed and generator-level value) and the solid line is the fit result.

```

/**
 * Generate reconstructed event from generator-level event
 * that needs to be already filled when calling this function.
 *
 * @param[in,out] event Event.
 */
virtual void generate_event(void *event) = 0;

```

The event class should contain both generator-level and reconstructed kinematic information. For other types of fits, the user needs to implement loading of maximum density which is used for normalization and the density function itself.

```

/**
 * Load maximum density.
 *
 * @param[in] fit_name Fit name.
 *
 * @return Zero on success, non-zero value on error.
 */
virtual int load_maximum_density(const char *fit_name) = 0;

/**
 * Calculate density function normalized so that its maximum value
 * is less than or equal to 1.
 *
 * @param[in] event Event.
 */
virtual double density(const void *event) = 0;

```

The density function can be implemented by calling the density used by the fit with a choice of the necessary function if the model has multiple ones selecting the necessary process, channel, and data sample.

#### 7.4. Background fit and template sources

The background is parameterized by a seven-dimensional second-order polynomial:

$$B(\Phi) = P_2(\Phi). \quad (77)$$

Projections of background fit results onto  $M_{K^{(1)}\pi^{(2)}}$ ,  $M_{\pi^{(1)}\pi^{(2)}}$ , and  $M_{K^{(1)}\pi^{(1)}\pi^{(2)}}$  for the energy point  $\sqrt{s} = 2000$  MeV are shown in Fig. 4.

The density functions are similar but not necessarily the same for different models. They may also depend on the process (i.e.  $e^+e^- \rightarrow K^+K^-\pi^+\pi^-$  or  $e^+e^- \rightarrow K_S^0K_S^0\pi^+\pi^-$ ), experimental period, data sample, and decay channel. There is no dependency on experimental period and no different decay channels in the  $e^+e^- \rightarrow K\bar{K}\pi\pi$  example. The source files are implemented as templates. During building, a different source file is generated for each

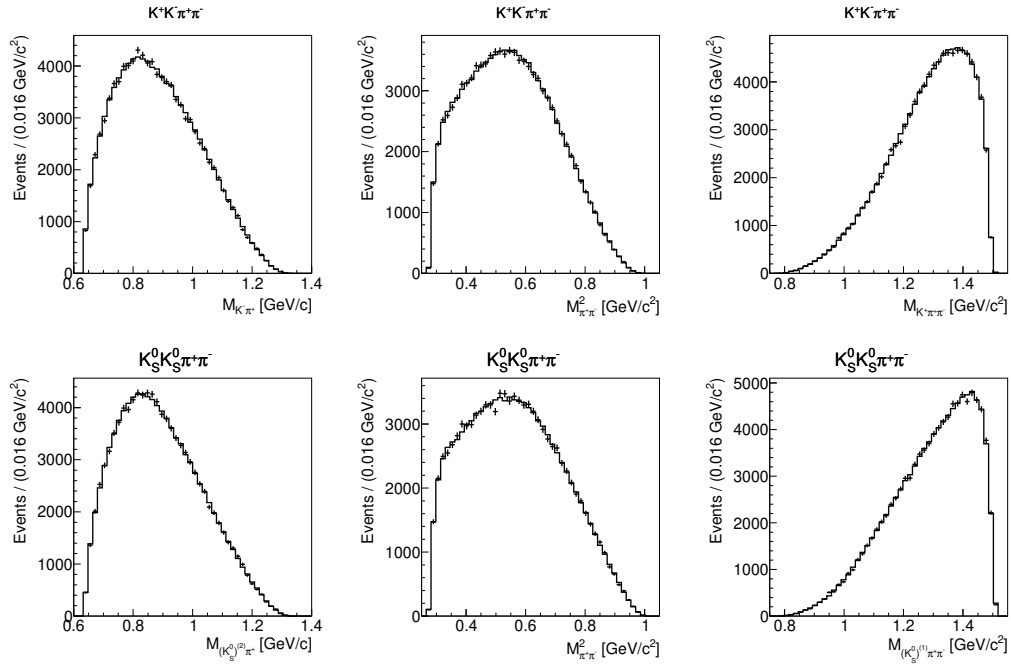


Figure 4: Projections of background fit results onto  $M_{K^{(1)}\pi^{(2)}}$ ,  $M_{\pi^{(1)}\pi^{(2)}}$ , and  $M_{K^{(1)}\pi^{(1)}\pi^{(2)}}$  for the energy point  $\sqrt{s} = 2000$  MeV. The points with error bars are data and the solid line is the fit result.

necessary variant. The sources for all models are collected by calling CMAKE function

```
function(vecampfit_collect_model_sources amplitude fit_types process_groups
        model_lists models dependencies get_fit_type_sources_1
        get_process_sources_1 get_model_sources_1 get_model_process_sources_1
        get_submodel_sources get_model_process_sources_2 get_model_sources_2
        get_process_sources_2 get_fit_type_sources_2)
```

where the arguments `get*` are CMAKE functions returning the lists of generated sources, header files, and generation targets. For example, the generation of the background-density source files is performed in the function `get_submodel_sources` by

```
vecampfit_template_source_model_process_sample (
    ${amplitude} ${process_group} ${model_list} ${model_name} ${process}
    ${sample} ${fit_type}_density.F90 " " "vecampfit/examples"
    "${include_directories}" FALSE FALSE " " " " " "
    generated_sources_2 generation_targets_2
)
```

The generation is performed by AWK script `awk/analysis_template_source.awk`. For example, the background-density function is declared as

```
MODULE SUBROUTINE BACKGROUND_DENSITY_#MODEL#_#PROCESS#_#SAMPLE#(BD, EV, PAR, &
&    PAR_BUF) BIND(C)
```

and for the default model for process  $e^+e^- \rightarrow K^+K^-\pi^+\pi^-$  at  $\sqrt{s} = 1800$  MeV this declaration expands into

```
MODULE SUBROUTINE BACKGROUND_DENSITY_kpkmpippim_default_kpkmpippim_1800_mev ( &
&    BD, EV, PAR, PAR_BUF) BIND(C)
```

Configuration of the model is performed by C preprocessor. For example, the background configuration header `config_background_kpkmpippim_default_1800_mev.h` for the same energy point contains the polynomial order only:

```
#ifndef VECAMPFIT_EXAMPLES_EPEM_KKPIPI_CONFIG_BACKGROUND_#MODEL#_#PROCESS#_#SAMPLE#_H
#define VECAMPFIT_EXAMPLES_EPEM_KKPIPI_CONFIG_BACKGROUND_#MODEL#_#PROCESS#_#SAMPLE#_H

// Configuration of background model for E = 1800 MeV.

// Polynomial order.
#define POLYNOMIAL_ORDER 2

#endif
```

First-level configuration headers are created manually for each model. Higher-level configuration headers include the original headers and provide other definitions based on the previous ones and also process, experimental period, data sample, and decay channel. Such headers are included from source files; similar to them, the configuration headers are templates created for

each necessary model variant. For background fit, the second-level header `configuration_background.h` contains common process-based definitions only:

```
#ifndef VECAMPFIT_EXAMPLES_EPEM_KKPIPI_CONFIGURATION_BACKGROUND_#MODEL#_#PROCESS#_#SAMPLE#_H
#define VECAMPFIT_EXAMPLES_EPEM_KKPIPI_CONFIGURATION_BACKGROUND_#MODEL#_#PROCESS#_#SAMPLE#_H

#include <vecampfit/examples/epem_kkpipi/models/#model#/#process#/#sample#/config_background.h>

// Configuration of background model.

// Process.
#include <vecampfit-example-models/epem_kkpipi/#process#/process.h>

#endif
```

Signal fit discussed in Sec. 7.5 provides more complex example of model configuration.

### 7.5. Signal fit and simultaneous fitting

VECAMPFIT supports simultaneous fitting of multiple data sets. Signal and background density function and event-buffer type, and background parameter-buffer type are set separately for each simultaneous-fit point. The fit parameters and signal parameter buffer are common for the entire fit. Typical scenarios for simultaneous fitting include different experimental periods with substantially different conditions such as Belle and Belle II; different but related amplitudes such as  $B$  decays with  $\psi(2S) \rightarrow e^+e^-$  or  $\mu^+\mu^-$  and  $\psi(2S) \rightarrow J/\psi\pi^+\pi^-$ , or with  $D^{*0} \rightarrow D^0\pi^0$  and  $D^{*0} \rightarrow D^0\gamma$ ; and fit to  $e^+e^-$  annihilation processes at multiple different energies, which is illustrated by the  $e^+e^- \rightarrow K\bar{K}\pi\pi$  example.

The signal fit is performed simultaneously for  $e^+e^- \rightarrow K^+K^-\pi^+\pi^-$  and  $e^+e^- \rightarrow K_S^0K_S^0\pi^+\pi^-$  at five different energy points: 1800, 1850, 1900, 1950, and 2000 MeV; thus, there are 10 simultaneous-fit points in total. The production amplitudes  $H_{\lambda_{K^{(1)}}0}^{(\gamma^* \rightarrow K_J^{(1)}\bar{K}^{(2)})}$  depend on the energy point, while the decay amplitudes such as  $H_{\lambda_{K_J^{(12)}}0}^{(K_J^{(1)} \rightarrow K_J^{*(12)}K^{(1)})}$  are common for all energy points.

Projections of signal fit results onto  $M_{K^{(1)}\pi^{(2)}}$ ,  $M_{\pi^{(1)}\pi^{(2)}}$ , and  $M_{K^{(1)}\pi^{(1)}\pi^{(2)}}$  for the energy point  $\sqrt{s} = 2000$  MeV are shown in Fig. 5.

VECAMPFIT provides a structure `vecampfit::simultaneous_fit_point` containing functions and class definitions depending on the simultaneous-fit point and fit-point process, experimental period, data sample, and channel.

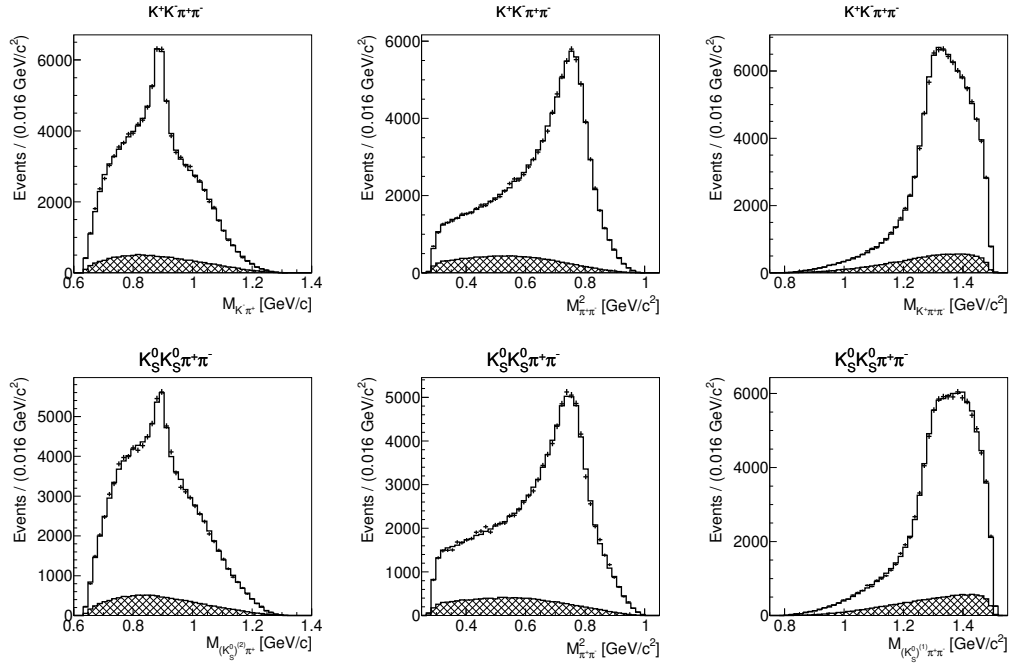


Figure 5: Projections of signal fit results onto  $M_{K^{(1)}\pi^{(2)}}$ ,  $M_{\pi^{(1)}\pi^{(2)}}$ , and  $M_{K^{(1)}\pi^{(1)}\pi^{(2)}}$  for the energy point  $\sqrt{s} = 2000$  MeV. The points with error bars are pseudo-data, the solid line is the fit result, and the dashed histogram is the background contribution.

A vector of simultaneous-fit point structures is declared in the signal fitting program as

```

const std::vector<vecampfit::simultaneous_fit_point> c_simultaneous_fit_points {
#if USE_KPKMPIPPIM && USE_SAMPLE_1800_MEV
    vecampfit::simultaneous_fit_point{
        epem_kkpi ::process::c_kpkmpippim, 1, 1, 1, false, {},
        {0, fill_signal_event_buffer_#model#_kpkmpippim,
         sizeof(seb_#model#_kpkmpippim), VECAMPFIT_FITTER_DENSITY_FUNCTION(
         signal_density_#model#_kpkmpippim_1800_mev)},
        {BACKGROUND_FRACTION_KPKMPIPPIM_1800_MEV,
         fill_background_event_buffer_kpkmpippim_default_kpkmpippim_1800_mev,
         sizeof(beb_kpkmpippim_default_kpkmpippim_1800_mev),
         VECAMPFIT_FITTER_FILL_PARAMETER_BUFFER_FUNCTION(
         fill_background_pb_kpkmpippim_default_kpkmpippim_1800_mev),
         sizeof(bpb_kpkmpippim_default_kpkmpippim_1800_mev),
         VECAMPFIT_FITTER_DENSITY_FUNCTION(
         background_density_kpkmpippim_default_kpkmpippim_1800_mev)},
        {}, {}},
#endif
    /* Other vector elements are omitted. */
}

```

The fitter initialization then requires simple loops over the simultaneous-fit-point vector which do not require further checks whether the point is included into the fit. For example, the functions are initialized by

```

int set_simultaneous_fit_point_functions()
{
    int res;
    std::string file_name, channel_string;
    for (size_t i = 0; i < c_simultaneous_fit_points.size(); ++i) {
        const vecampfit::simultaneous_fit_point& point
            = c_simultaneous_fit_points[i];
        int simultaneous_fit_point = i + 1;
        int background_source = 1;
        res = vecampfit_fitter_set_fill_signal_event_buffer(
            point.signal.fill_event_buffer,
            point.signal.sizeof_event_buffer,
            simultaneous_fit_point);
        if (res != 0)
            return -1;
        /* Further initialization is omitted. */
    }
}

```

## 8. Performance

### 8.1. Vector length and link-time optimization

Performance tests are carried out at two machines. The first one has an AMD Ryzen 3600 CPU with 6 cores and 12 threads operating at the frequency of 3.6 GHz, 32 GB of RAM, which is sufficient for all testing

programs, and an NVIDIA GeForce GT 710 GPU with 2 GB of memory, which is a very basic GPU that cannot be used for any real calculations, but it is still possible to use it for testing. The second test machine has an Intel Core i3-10105 CPU operating at the frequency of 3.7 GHz and 8 GB of RAM. Both test machines are running Debian 12. All tests are performed in SYSTEMD multi-user mode without any GUI running. VECAMP-FIT is compiled by GCC version 15.2.0 with maximum possible optimization, including fast optimization settings (`-Ofast` GCC flag), aggressive inlining settings (`-param inline-unit-growth=10000 -param max-inline-insns-auto=10000 -param large-function-growth=10000`), link-time optimization (LTO) (`-flto`), and native code (`-march=native`).

Dependence of the performance on the vector length is measured by execution of the  $D^0 \rightarrow K^- \pi^+ \pi^0$  example with both float and double floating-point types and all vector lengths from 1 to 32. Since the dependence of the performance on internal library settings is checked, the comparison is performed for time per event per function call to eliminate the variation of execution time caused by the varying number of the likelihood function calls. The number of events used for fitting is 1000000 normalization Monte Carlo events and 100000 signal pseudo-data events. One OPENMP thread is used. The results are shown in Fig. 6. Local minima are observed for the vector lengths proportional to the lengths of the largest vector register. For both test machines, there are four 64-bit numbers or eight 32-bit numbers in the 256-bit AVX registers.

Additional tests are performed to determine the position of the global minimum. The dependence of the execution time on the vector length is checked again for vector lengths proportional to the length of the AVX registers: 8 for single-precision calculations and 4 for double-precision calculations. To check the effect of link-time optimization, the same tests are also performed for the  $D^0 \rightarrow K^- \pi^+ \pi^0$  example compiled without link-time optimization. The results are shown in Fig. 7. The preferred vector length is proportional to the length of the largest vector register at the machine with a small integer machine-dependent coefficient. The preferred vector lengths and improvements over the scalar version for both test machines are listed in Table 1. The improvement of the optimal-length vectorized calculation with respect to the scalar version is somewhat less than the vector-register length, e.g. the improvement for double precision is 2.7 and 3.9 for the test machines 1 and 2, respectively, while an AVX register contains four double-precision numbers. Link-time optimization also results in a considerable improvement

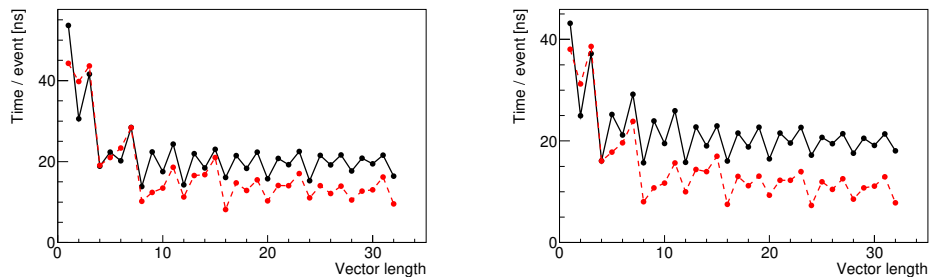


Figure 6: Dependence of the performance of the  $D^0 \rightarrow K^- \pi^+ \pi^0$  example on the vector length for test machine 1 (left) and 2 (right). The black solid line is the time per event per call for double-precision calculations (Fortran type `REAL(REAL64)`, C type `double`) and the red dashed line is the time per event for single-precision calculations (Fortran type `REAL(REAL32)`, C type `float`).

Table 1: Preferred vector length, improvement over scalar version, and effect of link-time optimization for the  $D^0 \rightarrow K^- \pi^+ \pi^0$  example. The time is per event per call in nanoseconds.

Machine	Test machine 1		Test machine 2	
	Single	Double	Single	Double
Preferred vector length	16	8	24	8
Scalar version time	44.3	53.6	38.0	43.1
Vector version time	8.23	13.9	7.37	15.8
Vector version time (no LTO)	9.50	24.9	9.77	21.1
Ratio of scalar and vector times	5.4	3.9	5.2	2.7
Ratio of (no LTO / LTO) times	1.5	1.8	1.3	1.3

for the optimal vector length: the fitting programs compiled with LTO are found to be from 1.3 to 1.8 times faster than the programs compiled without it. The LTO effect reduces for larger vector lengths which are non-optimal.

The dependence of the performance on the vector length for larger lengths is checked by performing a similar test with vector lengths proportional to 64 for double-precision calculations and 128 for single-precision calculations. The results are shown in Fig. 8. A slow increase of calculation time is observed for both single and double-precision calculations.

Based on the test results, the default set of vector lengths used when compiling the library is chosen to be equal to small powers of 2 and includes 1, 2, 4, 8, 16, 32, and 64.

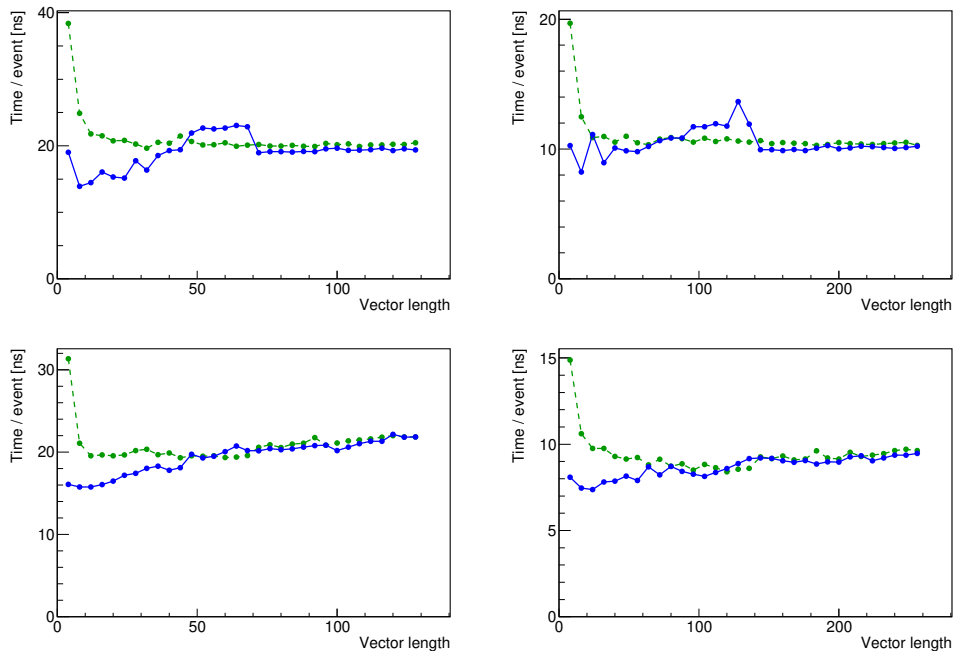


Figure 7: Dependence of the performance of the  $D^0 \rightarrow K^- \pi^+ \pi^0$  example on the vector length for double-precision calculations (left) and single-precision calculations (right) for test machine 1 (top) and 2 (bottom) for vector lengths proportional to the length of AVX registers (4 for double-precision calculations and 8 for single-precision calculations). The blue solid line is the time per event per call with LTO and the green dashed line is the time per event per without LTO.

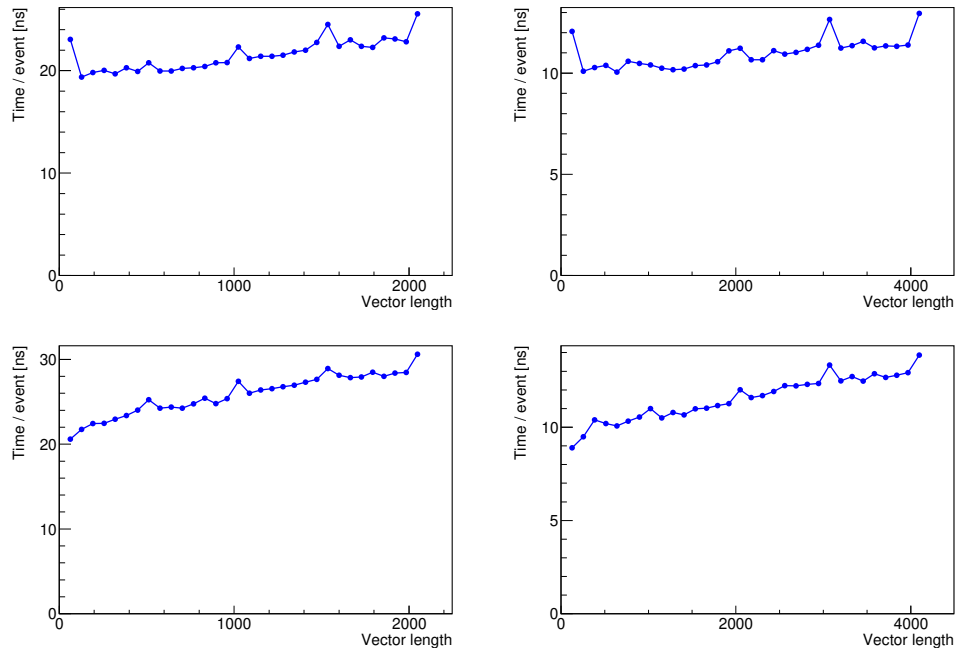


Figure 8: Dependence of the performance of the  $D^0 \rightarrow K^- \pi^+ \pi^0$  example on the vector length for double-precision calculations (left) and single-precision calculations (right) for test machine 1 (top) and 2 (bottom) for vector lengths proportional to 64 for double-precision calculations and 128 for single-precision calculations. The blue solid line is the time per event per call with LTO.

8.2. Comparison with an imperative-programming framework: LAURA<sup>++</sup>

LAURA<sup>++</sup> is a Dalitz-plot fitting library [13]. A dedicated example `laura_genfit3k` is implemented in VECAMPFIT to compare its performance with LAURA<sup>++</sup>. This example performs a Dalitz analysis of a simplified model of the decay  $B^+ \rightarrow K^+K^+K^-$ , reimplementing the LAURA<sup>++</sup> example `GenFit3K` as closely as possible. Exact reimplementaion is not possible as normalization of each individual resonance is performed in LAURA<sup>++</sup>, while VECAMPFIT does not provide any way to do the same. Thus, the resulting physical model is the same but the amplitude normalizations are different.

The amplitude is calculated using covariant formalism. Kinematic covariant factor for the decay chain  $0 \rightarrow R + 3$ ,  $R \rightarrow 1 + 2$  is given by

$$f(m_{12}) = \sqrt{1 + y^2} = \frac{m_0^2 + m_{12}^2 - m_3^2}{2m_{12}m_0}, \quad (78)$$

where  $m$  are invariant masses of particles or particle combinations specified by the subscript [58, 59]. Covariant factors for specific spins of intermediate resonances are

$$\begin{aligned} F_1^{(\text{cov})}(m_{12}) &= \sqrt{1 + y^2} = f, \\ F_2^{(\text{cov})}(m_{12}) &= \frac{3}{2} + y^2 = \frac{1}{2} + f^2, \\ F_3^{(\text{cov})}(m_{12}) &= \sqrt{1 + y^2} \left( \frac{5}{2} + y^2 \right) = f \left( \frac{3}{2} + f^2 \right), \\ F_4^{(\text{cov})}(m_{12}) &= \frac{35 + 40y^2 + 8y^4}{35} = \frac{3 + 24f^2 + 8f^4}{35}. \end{aligned} \quad (79)$$

The angular distribution depends on Legendre polynomials

$$\begin{aligned} P_0^{(\text{Leg})}(x) &= 1, \\ P_1^{(\text{Leg})}(x) &= x, \\ P_n^{(\text{Leg})}(x) &= \frac{1}{n} [(2n - 1)xP_{n-1}(x) - (n - 1)P_{n-2}(x)], \end{aligned} \quad (80)$$

which are normalized differently in LAURA<sup>++</sup>:

$$P_L^{(\text{Leg LAURA}^{++})}(x) = \frac{(-1)^L 2^{2L}}{\binom{2L}{L}} P_L^{(\text{Leg})}(x). \quad (81)$$

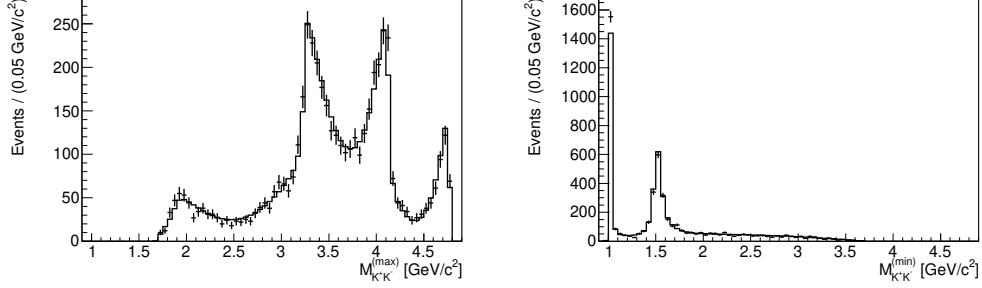


Figure 9: Results of fit to the  $B^+ \rightarrow K^+K^+K^-$  signal distribution for a pseudoexperiment generated by LAURA<sup>++</sup> example GenFit3K. The points with error bars are data, the solid line is the fit result, and the hatched histograms are the background contribution.

Full angular distribution for the decay chain  $0 \rightarrow R + 3$ ,  $R \rightarrow 1 + 2$  is given by

$$A_R^{(\text{ang})}(\Phi) = (p^*q)^L F_L^{(\text{cov})}(m_{12}) P_L^{(\text{Leg LAURA}^{++})}(\cos \theta_R), \quad (82)$$

where  $p^*$  is the momentum of the particle 3 in the rest frame of the particle 0,  $q$  is the momentum of the particles 1 and 2 in the rest frame of the intermediate resonance  $R$ , and  $\theta_R$  is the  $R$  helicity angle.

The amplitude of the decay chain  $B^+ \rightarrow \phi_J K^+$ ,  $\phi_J \rightarrow K^+ K^-$  is

$$A_{\phi_J}(\Phi) = B_{\phi_J}^{(\text{no } q)}(m) A_{\phi_J}^{(\text{ang})}(\Phi) F_{B^+}^{(BW)}(q(F_J^{(\text{cov})}(m_{12}))^{\frac{1}{J}}, r^{(B)}, J), \quad (83)$$

where the Blatt-Weisskopf formfactor with scaled momentum is used for the decay  $B^+ \rightarrow \phi_J K^+$  and  $r^{(B)}$  is  $B$  effective radius. The amplitude is

$$A(\Phi) = a_0 + \sum_R a_R \left[ A_R^{(B^+ \rightarrow \phi_J K_{(1)}^+)}(\Phi) + A_R^{(B^+ \rightarrow \phi_J K_{(2)}^+)}(\Phi) \right] \quad (84)$$

where  $a_0$  is constant nonresonant amplitude,  $a_R$  are resonance complex amplitudes, and symmetrization over two ways of selection of the decay chain is performed. The signal density function is  $S(\Phi) = |A(\Phi)|^2$ . Two intermediate resonances  $\phi(1020)$  and  $f_2'(1525)$  are included into the model. The background is not included. The VECAMPFIT example is able to use pseudoexperiments generated by LAURA<sup>++</sup> after conversion which stores each pseudoexperiment in an individual file. The fit results for a pseudoexperiment with 5000 signal events generated by LAURA<sup>++</sup> are shown in Fig. 9.

The VECAMPFIT example uses grid integration; the grid is manually set up to be exactly the same as the grid created by LAURA<sup>++</sup> automatically. Parallel calculations are implemented in LAURA<sup>++</sup> for independent data samples only, while VECAMPFIT is able to perform parallel calculations using different events from the same data sample. Thus, only one version of the LAURA<sup>++</sup> example is used for comparison; the calculations are performed in double precision by a single thread without vectorization. Similarly, one thread and double precision are used for VECAMPFIT; several different vector lengths are tested.

Similar to the LAURA<sup>++</sup> testing procedure [13], 50 pseudoexperiments are generated. LAURA<sup>++</sup> is compiled with maximum optimization (`-Ofast` GCC flag), native-code generation (`-march=native`), and link-time optimization (`-flto`). Unlike the previous performance tests, total execution time is used for comparison with other libraries, since they have different internal settings and available features. Initial values of the amplitudes are randomized for both LAURA<sup>++</sup> and VECAMPFIT. VECAMPFIT fit is performed in two versions with and without explicit gradient calculation.

It is checked whether the fits converge to the same minimum by comparing the resulting amplitudes. It is found that there is a second solution with approximately inverse amplitude of the  $f_2'(1525)$ . Both LAURA<sup>++</sup> and VECAMPFIT fits converge to the second solution for about 30% of fits. If they both converge to the main solution, then the results are the same.

The results are listed in Table 2. The VECAMPFIT fit is about 4 to 5 times faster than LAURA<sup>++</sup> fit on both test machines, although note that a part of this difference is caused by different normalization in LAURA<sup>++</sup> requiring more calculations. Usage of gradient calculation reduces the fitting time further, but the effect is not very large because this is a simple fit with only 10 free parameters. Although the considered  $B^+ \rightarrow K^+ K^+ K^-$  model is very simple, runs fast, and does not require much optimization, the performed comparison also estimates possible improvement from vectorization and gradient calculation in more complex analyses. While VECAMPFIT fit is faster, it is more difficult to implement due to the requirement of manual implementation of vectorization and gradient calculation.

### 8.3. Comparison with a declarative-programming framework: TENSORFLOW-ANALYSIS2

TENSORFLOWANALYSIS2 (TFA2) is an amplitude-analysis framework based on TENSORFLOW [17]. It does not have any tagged releases; the de-

Table 2: Comparison of fitting time of the  $B^+ \rightarrow K^+K^+K^-$  example for VECAMPFIT and LAURA<sup>++</sup> implementations. The time is the total clock fitting time of 50 pseudoexperiments in seconds. The ratios of LAURA<sup>++</sup> and VECAMPFIT time and VECAMPFIT times with and without gradient is calculated for the optimal VECAMPFIT vector length.

Machine	Machine 1	Machine 2
Generation (LAURA <sup>++</sup> )	176	130
LAURA <sup>++</sup>	1526	1235
VECAMPFIT, vector length 4	322	314
VECAMPFIT, vector length 8	303	313
VECAMPFIT, vector length 16	327	347
VECAMPFIT, vector length 32	346	333
VECAMPFIT, vector length 64	322	314
VECAMPFIT, gradient, vector length 4	222	203
VECAMPFIT, gradient, vector length 8	225	200
VECAMPFIT, gradient, vector length 16	244	218
VECAMPFIT, gradient, vector length 32	268	229
VECAMPFIT, gradient, vector length 64	223	203
LAURA <sup>++</sup> / VECAMPFIT without gradient	5.0	3.9
LAURA <sup>++</sup> / VECAMPFIT with gradient	6.9	6.2
VECAMPFIT (without / with gradient)	1.36	1.57

velopment version with git commit ccae92f043 performed in October 2023 is used for performance comparison. TENSORFLOW version 2.17.0 and IMINUIT 2.30.0 are used for function evaluation and minimization, respectively. Comparison between VECAMPFIT and TFA2 is performed using the  $D^0 \rightarrow K^-\pi^+\pi^0$  example with 50 different pseudoexperiments of 100000 events each and a common normalization sample consisting of 1000000 events. The example is reimplemented using TFA2, and the pseudoexperiments are fitted with both VECAMPFIT and TFA2 fitting programs with random initial values of the amplitudes. The bufferization and parameter-releasing sequence are the same for VECAMPFIT and TFA2 fits. Note that the masses and widths of all resonances can be released, thus, amplitudes of individual resonances cannot be added to the event buffer.

By default, TENSORFLOW sets the number of threads to the number of CPU threads to achieve its maximum usage. This configuration is used for testing. It is equivalent to OPENMP behavior if the number of threads is not set explicitly. Due to the need of GPU offloading, comparisons of VECAMPFIT and TFA2 are performed at the test machine 1 only. By default, gradient is enabled for TFA2 because it is computed automatically and disabled for VECAMPFIT since it requires manual implementation, but both versions with and without gradient calculation are tested for both frameworks. TFA2 fit without JIT compilation is very slow on CPU; one test without JIT is performed for comparison but the others are performed using JIT. Versions with free amplitudes only and additional releasing of masses or masses and widths are tested. Summary of performance tests is shown in Table 3. Explicit gradient calculation reduces the total CPU time, but for TFA2 it does not always improve the clock time. The ratios of best TFA2 and VECAMPFIT fitting times are shown in Table 4. For all fits, VECAMPFIT is more than an order of magnitude faster.

Finally, VECAMPFIT and TFA2 fitting times are compared for the case of GPU offloading. CUDA version 11.4.4 and CUDNN version 8.7.0 are used by TFA2 for running at GPU. Due to the limited performance of the available GPU, the number of pseudoexperiments used for comparison is reduced from 50 to 5, the number of events in each pseudoexperiment is reduced from 100000 to 20000, and the number of events in the normalization sample is reduced from 1000000 to 200000. The total amount of calculations required for GPU test is 50 times less than the CPU one. JIT compilation improves TFA2 fitting time on GPU, but the difference is much smaller than on CPU. However, fits with JIT compilation require more memory and

Table 3: Comparison of fitting time of the  $D^0 \rightarrow K^- \pi^+ \pi^0$  example for VECAMPFIT and TFA2 implementations. VECAMPFIT fit is performed in double precision with vector length 4. The clock and CPU times are in seconds and maximum memory usage is in megabytes. The GPU fits perform 50 times less calculations than CPU fits.

Test	Clock time	CPU time	Memory
VECAMPFIT	262	2278	490
VECAMPFIT, free $m$	430	4339	490
VECAMPFIT, free $m, \Gamma$	513	5249	490
VECAMPFIT, gradient	209	1679	490
VECAMPFIT, gradient, free $m$	298	2750	490
VECAMPFIT, gradient, free $m, \Gamma$	274	2450	490
TFA2, no JIT	6387	67173	4954
TFA2, JIT, no gradient	2762	8410	1544
TFA2, JIT, no gradient, free $m$	4610	14451	1808
TFA2, JIT, no gradient, free $m, \Gamma$	5622	17825	1799
TFA2, JIT	3464	7750	4836
TFA2, JIT, free $m$	5243	12124	4857
TFA2, JIT, free $m, \Gamma$	5557	13186	4928
VECAMPFIT, GPU	5231	5228	377
VECAMPFIT, GPU, free $m$	10516	10515	366
VECAMPFIT, GPU, free $m, \Gamma$	11622	11621	366
TFA2, GPU, no JIT	634	648	1756
TFA2, GPU, no JIT, free $m$	1152	1168	1877
TFA2, GPU, no JIT, free $m, \Gamma$	1217	1230	1872
TFA2, GPU, JIT	516	525	2425

Table 4: Ratios of TFA2 and VECAMPFIT fitting times for the  $D^0 \rightarrow K^- \pi^+ \pi^0$  example. The fits with free amplitudes, free amplitudes and masses, and free amplitudes, masses, and widths have 15, 20, and 25 free parameters, respectively.

Free parameters	CPU	GPU
Amplitudes	13.2	0.12
Amplitudes, $m$	15.4	0.11
Amplitudes, $m, \Gamma$	20.3	0.10

cannot be executed due to insufficient GPU memory size, thus, fits without JIT are used for comparison. Vector length is equal to one for VECAMPFIT because of a GCC issue resulting in incorrect results when using OPENACC vector loops explicitly. This limits VECAMPFIT offloading performance and currently prevents its usage for data analysis with GPU offloading. The performance-comparison results are opposite to CPU: TFA2 performs much better and runs about an order of magnitude faster.

## 9. Conclusions

A new library VECAMPFIT has been developed to perform amplitude analyses of various processes in high-energy physics. It is designed to achieve high performance of the analysis code by vectorization of data storage and amplitude calculations and provides a number of vectorized subroutines for physical quantities and mathematical functions. The fitter supports explicit gradient calculation. Simultaneous fitting of multiple data sets with related amplitudes is possible. Specific tests have been carried out to compare VECAMPFIT performance with an existing imperative-programming fitting framework (LAURA<sup>++</sup>) and a declarative-programming framework (TENSORFLOWANALYSIS2) and show a major improvement compared to both at CPU. However, TENSORFLOWANALYSIS2 performs much better for GPU offloading; offloading support is experimental in VECAMPFIT and is planned to be improved in future releases.

## References

- [1] R. Aaij, et al., Determination of the  $X(3872)$  meson quantum numbers, *Phys. Rev. Lett.* 110 (2013) 222001. [arXiv:1302.6269](#), [doi:10.1103/PhysRevLett.110.222001](#).
- [2] R. Aaij, et al., Quantum numbers of the  $X(3872)$  state and orbital angular momentum in its  $\rho^0 J/\psi$  decay, *Phys. Rev. D* 92 (1) (2015) 011102. [arXiv:1504.06339](#), [doi:10.1103/PhysRevD.92.011102](#).
- [3] K. Chilikin, et al., Experimental constraints on the spin and parity of the  $Z(4430)^+$ , *Phys. Rev. D* 88 (7) (2013) 074026. [arXiv:1306.4894](#), [doi:10.1103/PhysRevD.88.074026](#).

- [4] R. Aaij, et al., Observation of the resonant character of the  $Z(4430)^-$  state, *Phys. Rev. Lett.* 112 (22) (2014) 222002. [arXiv:1404.1903](#), [doi:10.1103/PhysRevLett.112.222002](#).
- [5] R. Aaij, et al., Observation of  $J/\psi\phi$  structures consistent with exotic states from amplitude analysis of  $B^+ \rightarrow J/\psi\phi K^+$  decays, *Phys. Rev. Lett.* 118 (2) (2017) 022003. [arXiv:1606.07895](#), [doi:10.1103/PhysRevLett.118.022003](#).
- [6] R. Aaij, et al., Observation of New Resonances Decaying to  $J/\psi K^+$  and  $J/\psi\phi$ , *Phys. Rev. Lett.* 127 (8) (2021) 082001. [arXiv:2103.01803](#), [doi:10.1103/PhysRevLett.127.082001](#).
- [7] A. Garmash, et al., Amplitude analysis of  $e^+e^- \rightarrow \Upsilon(nS)\pi^+\pi^-$  at  $\sqrt{s} = 10.865 \sim \text{GeV}$ , *Phys. Rev. D* 91 (7) (2015) 072003. [arXiv:1403.0992](#), [doi:10.1103/PhysRevD.91.072003](#).
- [8] R. Fletcher, A new approach to variable metric algorithms, *Comput. J.* 13 (3) (1970) 317–322. [doi:10.1093/comjnl/13.3.317](#).
- [9] F. James, M. Roos, Minuit: A System for Function Minimization and Analysis of the Parameter Errors and Correlations, *Comput. Phys. Commun.* 10 (1975) 343–367. [doi:10.1016/0010-4655\(75\)90039-9](#).
- [10] L. Dagum, R. Menon, OpenMP: an industry standard API for shared-memory programming, *IEEE Computational Science and Engineering* 5 (1) (1998) 46–55. [doi:10.1109/99.660313](#).
- [11] E. Gabriel, G. E. Fagg, G. Bosilca, T. Angskun, J. J. Dongarra, J. M. Squyres, V. Sahay, P. Kambadur, B. Barrett, A. Lumsdaine, R. H. Castain, D. J. Daniel, R. L. Graham, T. S. Woodall, Open MPI: Goals, Concept, and Design of a Next Generation MPI Implementation, in: *Proceedings, 11th European PVM/MPI Users' Group Meeting, Budapest, Hungary, 2004*, pp. 97–104.
- [12] R. Farber, *Parallel Programming with OpenACC*, Morgan Kaufmann, 2017.
- [13] J. Back, et al., LAURA<sup>++</sup>: A Dalitz plot fitter, *Comput. Phys. Commun.* 231 (2018) 198–242. [arXiv:1711.09854](#), [doi:10.1016/j.cpc.2018.04.017](#).

- [14] M. Shepherd, J. Stevens, R. Mitchell, M. Albrecht, B. Grube, A. Austregesilo, N. D. Hoffman, NilsHuesken, mashephe/amptools: Version 0.15.3 (Apr. 2024). doi:10.5281/zenodo.10961168.  
URL <https://doi.org/10.5281/zenodo.10961168>
- [15] PAWIAN.  
URL <https://gitlab.ep1.rub.de/pwa/Pawian>
- [16] M. Abadi, A. Agarwal, P. Barham, E. Brevdo, Z. Chen, C. Citro, G. S. Corrado, A. Davis, J. Dean, M. Devin, S. Ghemawat, I. Goodfellow, A. Harp, G. Irving, M. Isard, Y. Jia, R. Jozefowicz, L. Kaiser, M. Kudlur, J. Levenberg, D. Mané, R. Monga, S. Moore, D. Murray, C. Olah, M. Schuster, J. Shlens, B. Steiner, I. Sutskever, K. Talwar, P. Tucker, V. Vanhoucke, V. Vasudevan, F. Viégas, O. Vinyals, P. Warden, M. Wattenberg, M. Wicke, Y. Yu, X. Zheng, TensorFlow: Large-scale machine learning on heterogeneous systems, software available from tensorflow.org (2015).  
URL <http://tensorflow.org/>
- [17] TensorFlowAnalysis2.  
URL <https://github.com/apoluekt/TFA2>
- [18] Y. Jiang, Amplitude analysis tools at BESIII, Nuovo Cim. C 47 (4) (2024) 203. doi:10.1393/ncc/i2024-24203-0.
- [19] M. Fritsch, M. Michel, S. Pflüger, R. de Boer, L. Woltenberg, W. Gradl, P. Weidenkaff, K. Peters, K. Götzen, Common Partial Wave Analysis: A collaboration-independent organisation for amplitude analysis (Jul. 2022). doi:10.5281/zenodo.6908150.  
URL <https://doi.org/10.5281/zenodo.6908150>
- [20] J. Bradbury, R. Frostig, P. Hawkins, M. J. Johnson, C. Leary, D. Maclaurin, G. Necula, A. Paszke, J. VanderPlas, S. Wanderman-Milne, Q. Zhang, JAX: composable transformations of Python+NumPy programs (2018).  
URL <http://github.com/jax-ml/jax>
- [21] C. R. Harris, K. J. Millman, S. J. van der Walt, R. Gommers, P. Virtanen, D. Cournapeau, E. Wieser, J. Taylor, S. Berg, N. J. Smith,

- R. Kern, M. Picus, S. Hoyer, M. H. van Kerkwijk, M. Brett, A. Haldane, J. F. del Río, M. Wiebe, P. Peterson, P. Gérard-Marchant, K. Shepard, T. Reddy, W. Weckesser, H. Abbasi, C. Gohlke, T. E. Oliphant, Array programming with NumPy, *Nature* 585 (7825) (2020) 357–362. doi:10.1038/s41586-020-2649-2.  
URL <https://doi.org/10.1038/s41586-020-2649-2>
- [22] AmpGen, <https://github.com/GooFit/AmpGen>.
- [23] P. d’Argent, T. Evans, phdargen/AmpGen-B2VPPP:  $B \rightarrow \psi(2S)K\pi\pi$  analysis code (May 2024). doi:10.5281/zenodo.11212410.  
URL <https://doi.org/10.5281/zenodo.11212410>
- [24] R. Aaij, et al., Amplitude analysis of  $B^+ \rightarrow \psi(2S)K^+\pi^+\pi^-$  decays, *JHEP* 01 (2025) 054. arXiv:2407.12475, doi:10.1007/JHEP01(2025)054.
- [25] T. Abe, et al., Belle II Technical Design Report (11 2010). arXiv:1011.0352.
- [26] A. Abashian, et al., The Belle Detector, *Nucl. Instrum. Meth. A* 479 (2002) 117–232. doi:10.1016/S0168-9002(01)02013-7.
- [27] J. Brodzicka, et al., Physics Achievements from the Belle Experiment, *PTEP* 2012 (2012) 04D001. arXiv:1212.5342, doi:10.1093/ptep/pts072.
- [28] R. Brun, F. Rademakers, ROOT: An object oriented data analysis framework, *Nucl. Instrum. Meth. A* 389 (1997) 81–86. doi:10.1016/S0168-9002(97)00048-X.
- [29] S. Kopp, et al., Dalitz analysis of the decay  $D^0 \rightarrow K^-\pi^+\pi^0$ , *Phys. Rev. D* 63 (2001) 092001. arXiv:hep-ex/0011065, doi:10.1103/PhysRevD.63.092001.
- [30] J. Blatt, V. Weisskopf, *Theoretical Nuclear Physics*, John Wiley & Sons, New York, 1952.
- [31] L. Fousse, G. Hanrot, V. Lefèvre, P. Pélissier, P. Zimmermann, MPFR: A multiple-precision binary floating-point library with correct rounding, *ACM Trans. Math. Softw.* 33 (2) (2007) 13–es. doi:10.1145/1236463.1236468.  
URL <https://doi.org/10.1145/1236463.1236468>

- [32] D. Harvey, P. Zimmermann, Short Division of Long Integers, in: Proceedings of the 20th Symposium on Computer Arithmetic (ARITH-20), 2011. doi:10.1109/ARITH.2011.11.
- [33] K. Petras, On the computation of the Gauss–Legendre quadrature formula with a given precision, *Journal of Computational and Applied Mathematics* 112 (1999) 253. doi:10.1016/S0377-0427(99)00225-3.
- [34] P. Tchébychev, Théorie des mécanismes connus sous le nom de parallélogrammes, *Mémoires présentés a l’Académie Impériale des sciences de St.-Petersbourg* 7 (1854) 539–568.
- [35] G. Källén, *Elementary particle physics*, Addison-Wesley, Reading, MA, 1964.
- [36] E. Anderson, Z. Bai, C. Bischof, L. S. Blackford, J. Demmel, J. J. Dongarra, J. Du Croz, S. Hammarling, A. Greenbaum, A. McKenney, D. Sorensen, *LAPACK Users’ guide* (third ed.), Society for Industrial and Applied Mathematics, USA, 1999.
- [37] A. C. Genz, A. A. Malik, Remarks on algorithm 006: An adaptive algorithm for numerical integration over an  $n$ -dimensional rectangular region, *Journal of Computational and Applied Mathematics* 6 (4) (1980) 295. doi:10.1016/0771-050X(80)90039-X.
- [38] G. J. Feldman, R. D. Cousins, A Unified approach to the classical statistical analysis of small signals, *Phys. Rev. D* 57 (1998) 3873–3889. arXiv:physics/9711021, doi:10.1103/PhysRevD.57.3873.
- [39] M. Shilling, Multivariate Two-Sample Tests Based on Nearest Neighbors, *J. Am. Stat. Assoc.* 81 (395) (1986) 799–806. doi:10.2307/2289012.
- [40] N. Henze, A Multivariate Two-Sample Test Based on the Number of Nearest Neighbor Type Coincidences, *Ann. Stat.* 16 (2) (1988) 772–783. doi:10.1214/aos/1176350835.
- [41] S. U. Chung, J. Brose, R. Hackmann, E. Klempt, S. Spanier, C. Strassburger, Partial wave analysis in K matrix formalism, *Annalen Phys.* 4 (1995) 404–430. doi:10.1002/andp.19955070504.

- [42] S. Navas, et al., Review of particle physics, Phys. Rev. D 110 (3) (2024) 030001. doi:10.1103/PhysRevD.110.030001.
- [43] S. M. Flatte, Coupled-Channel Analysis of the  $\pi\eta$  and  $K\bar{K}$  Systems Near  $K\bar{K}$  Threshold, Phys. Lett. B 63 (1976) 224–227. doi:10.1016/0370-2693(76)90654-7.
- [44] E. Wigner, Gruppentheorie und ihre Anwendungen auf die Quantenmechanik der Atomspektren, Friedr.Vieweg & Sohn, Braunschweig, 1931.
- [45] F. James, Monte-Carlo phase space, CERN-68-15 (5 1968).
- [46] P. A. Zyla, et al., Review of Particle Physics, PTEP 2020 (8) (2020) 083C01. doi:10.1093/ptep/ptaa104.
- [47] R. L. Workman, et al., Review of Particle Physics, PTEP 2022 (2022) 083C01. doi:10.1093/ptep/ptac097.
- [48] J. P. Lees, et al., Cross Sections for the Reactions  $e^+e^- \rightarrow K^+K^-\pi^+\pi^-$ ,  $K^+K^-\pi^0\pi^0$ , and  $K^+K^-K^+K^-$  Measured Using Initial-State Radiation Events, Phys. Rev. D 86 (2012) 012008. arXiv:1103.3001, doi:10.1103/PhysRevD.86.012008.
- [49] D. N. Shemyakin, et al., Measurement of the  $e^+e^- \rightarrow K^+K^-\pi^+\pi^-$  cross section with the CMD-3 detector at the VEPP-2000 collider, Phys. Lett. B 756 (2016) 153–160. arXiv:1510.00654, doi:10.1016/j.physletb.2016.02.072.
- [50] M. Ablikim, et al., Cross sections for the reactions  $e^+e^- \rightarrow K^+K^-\pi^+\pi^-(\pi^0)$ ,  $K^+K^-K^+K^-(\pi^0)$ ,  $\pi^+\pi^-\pi^+\pi^-(\pi^0)$ ,  $p\bar{p}\pi^+\pi^-(\pi^0)$  in the energy region between 3.773 and 4.600 GeV, Phys. Rev. D 104 (11) (2021) 112009. arXiv:2109.12751, doi:10.1103/PhysRevD.104.112009.
- [51] J. P. Lees, et al., Cross sections for the reactions  $e^+e^- \rightarrow K_S^0K_L^0$ ,  $K_S^0K_L^0\pi^+\pi^-$ ,  $K_S^0K_S^0\pi^+\pi^-$ , and  $K_S^0K_S^0K^+K^-$  from events with initial-state radiation, Phys. Rev. D 89 (9) (2014) 092002. arXiv:1403.7593, doi:10.1103/PhysRevD.89.092002.

- [52] R. R. Akhmetshin, et al., Study of the process  $e^+e^- \rightarrow K_S^0 K_S^0 \pi^+ \pi^-$  in the c.m. energy range 1.6–2.0 GeV with the CMD-3 detector, *Phys. Lett. B* 804 (2020) 135380. [arXiv:1912.05751](#), [doi:10.1016/j.physletb.2020.135380](#).
- [53] R. Aaij, et al., Studies of the resonance structure in  $D^0 \rightarrow K^\mp \pi^\pm \pi^\pm \pi^\mp$  decays, *Eur. Phys. J. C* 78 (6) (2018) 443. [arXiv:1712.08609](#), [doi:10.1140/epjc/s10052-018-5758-4](#).
- [54] M. Jacob, G. C. Wick, On the General Theory of Collisions for Particles with Spin, *Annals Phys.* 7 (1959) 404–428. [doi:10.1016/0003-4916\(59\)90051-X](#).
- [55] S. Agostinelli, et al., GEANT4—a simulation toolkit, *Nucl. Instrum. Meth. A* 506 (2003) 250–303. [doi:10.1016/S0168-9002\(03\)01368-8](#).
- [56] J. Allison, et al., Geant4 developments and applications, *IEEE Trans. Nucl. Sci.* 53 (2006) 270. [doi:10.1109/TNS.2006.869826](#).
- [57] J. Allison, et al., Recent developments in Geant4, *Nucl. Instrum. Meth. A* 835 (2016) 186–225. [doi:10.1016/j.nima.2016.06.125](#).
- [58] V. Filippini, A. Fontana, A. Rotondi, Covariant spin tensors in meson spectroscopy, *Phys. Rev. D* 51 (1995) 2247–2261. [doi:10.1103/PhysRevD.51.2247](#).
- [59] R. Aaij, et al., Dalitz plot analysis of  $B^0 \rightarrow \overline{D}^0 \pi^+ \pi^-$  decays, *Phys. Rev. D* 92 (3) (2015) 032002. [arXiv:1505.01710](#), [doi:10.1103/PhysRevD.92.032002](#).